Electronic Supplementary Material (ESI) for Nanoscale.

Supplementary Information

Copper Single-Site Engineering in MOF-808 Membranes for Improved Water Treatment

Isabel del Castillo-Velilla,[a] Ignacio Romero-Muñiz,[a] Carlo Marini,[b] Carmen Montoro[a,c*] and Ana Eva Platero-Prats [a,d*]

[a] Departamento de Química Inorgánica, Facultad de Ciencias, Universidad Autónoma de Madrid, 28049 Madrid, Spain.

[b] CELLS – ALBA Synchrotron Radiation Facility, Carrer de la Llum 2-26, 08090, Cerdanyola del Vallès, Barcelona, Catalonia, Spain.

[c] Institute for Advanced Research in Chemical Sciences (IAdChem), Universidad Autónoma de Madrid, 28049 Madrid, Spain.

[d] Condensed Matter Physics Center (IFIMAC), Universidad Autónoma de Madrid, 28049 Madrid, Spain.

Table of Contents

S1. Synthesis of the materials and membranes

All chemicals and reagents were used as received without further purification. $ZrOCl_2 \cdot 8H_2O$, trimesic acid, and polyvinyl fluoride (PVDF) (Mw ~ 180,000) were purchased from Sigma-Aldrich. Formic acid, methanol, and *N, N*-dimethylformamide (DMF) were obtained from Carlo Erba, $Cu(CH_3CO_2)_2 \cdot H_2O$ from Prolabo, and tyrosol (TyrOH) (2-(4-Hydroxyphenyl) ethanol) from Fluorochem.

Synthesis of MOF-808 nanoparticles (NPs)

MOF-808 NPs. They were synthesized by modification of the reported conditions.[1] An optimized microwave-assisted synthesis was used to achieve the desired particle size and crystallinity (Table S1.1). Briefly, trimesic acid or 1, 3, 5-benzenetricarboxylic acid (BTC) (42 mg, 0.20 mmol) and $ZrOCl_2 \cdot 8H_2O$ (194 mg, 0.60 mmol) were added to a mixture of 9 mL of formic acid (4.5 mL) and DMF (4.5 mL) in a microwave tube. The reaction was heated at 130 °C for the selected time (30, 45, 60, 75, or 90 min) in an Advanced Microwave Digestion Labstation (Milestone - ETHOS 1). After cooling down to room temperature, the reaction mixture was centrifuged in a Hettich MIKRO 200 centrifuge (2 min, 12000 rpm), and the solid was washed with DMF, distilled water, and methanol (3 times with 30 mL each). The resulting mixture was kept in fresh methanol to avoid aggregation, yielding a white suspension of MOF-808 NPs (130 mg dried, 53 % yield). ^{1}H-NMR (Figure S2.1): 8.60 (s, 6H, 2 × BTCs); 8.06 (s, 1H, 1 × COOH). $[Zr_6O_8H_4(C_9H_3O_6)_2(COOH)(H_2O)_5(OH)_5]$.

Table S1.1. Reaction conditions and results for the synthesis of MOF-808 NPs at 130 ºC.

Heating time*[a] / *min	***Yield* / *%***	***Particle size*[b] / *nm***
30	11	500
45	53	130
60	23	400
75	49	200
90	40	120

[a] 45 mins was the optimal time considering the crystallinity of the products (see Figure S7.1).
[b] Average particle size observed by TEM or FE-SEM (see S3 and S4 sections).

Cu-MOF-808 NPs. The metalation of MOF-808 NPs was obtained following the procedure already reported by us[2] where MOF-808 NPs (100 mg, 0.056 mmol), $Cu(CH_3COO)_2 \cdot H_2O$ (68 mg, 0.34 mmol), and methanol (10 mL) were placed in a sealed vial stirred at 60 °C overnight. After cooling to room temperature, the reaction mixture was centrifuged, and the solid was washed with methanol, distilled water, and ethanol (3 times with 10 mL each). The resulting mixture was kept in fresh ethanol, for avoiding aggregation, yielding a blue suspension of Cu-MOF-808 NPs (80 mg dried, 80 % yield). ICP analysis, ratio Cu/Zr_6: 3.1 $[Zr_6Cu_{3.1}O_8H_4(C_9H_3O_6)_2(OH)_{9.8}(H_2O)_{3.1}(C_2H_3O_2)_{2.4}]$.^{1}H-NMR (Figure S2.1): 8.60 (s, 6H, 2 × BTCs), 1.89 (s, 7.3H, 2.4 x acetate).

Membrane preparation

All membranes had a diameter of 0.045 m (A = 0.002 m^2) (Figure S1.1). An optimization process was carried out for the preparation of the membranes changing both parameters the time of drying and the temperature (Table S1.2).

Table S1.2. Casting conditions and results for the preparation of the MMMs.

Drying time / h	***Temperature / ºC***	***Observations***
3	80	Flat but too porous, low yields for catalysis
16	60	Bending difficulties
16	45	Dense and flat, high yields for catalysis

PVDF membrane. PVDF pellets were dried at 80 °C for 24 h to remove moisture. A solution of 5 wt% PVDF in DMF (320 mg of PVDF in 6.9 mL of DMF) was prepared at 60 °C for 2 h. Then, the solution was cast onto a Petri dish and dried at 45 ºC in an oven for 16 h followed by 2 h at 65 ºC yielding a white flexible membrane. Finally, the PVDF membrane was dried at 100 ºC for 30 mins in the oven, to remove all the solvent molecules before its use.

MMM preparation. MOF-808@PVDF and Cu-MOF-808@PVDF MMMs were prepared as follows. 15 wt% MOF NPs (55 mg) were suspended in DMF (6.9 mL) and placed in a sealed vial. The mixtures were stirred and sonicated until the NPs were homogeneously dispersed in the solvent. Then, 320 mg of PVDF (5 wt%) were added to the vials and the resulting solutions were stirred at 60 °C for 2 h until homogeneous suspensions with the NPs. The suspensions were cast onto a Petri dish and dried at 45 ºC for 16 h in the oven, followed by 2 h at 65 ºC yielding a white or blue flexible membrane depending on the NPs used. Finally, the MMMs were immersed in water for 30 mins, to remove all the solvent molecules before their use. In the case of the Cu-MOF-808@PVDF MMM, a change from blue to green colour could be observed during the heating, due to the water molecules loss.

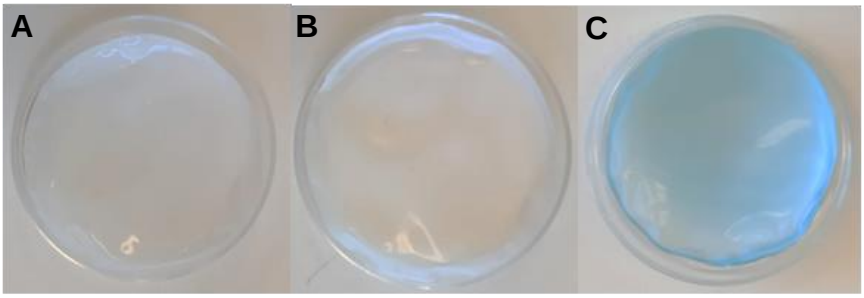

Figure S1.1. Pictures of the (A) PVDF, (B) MOF-808@PVDF, and (C) Cu-MOF-808@PVDF membranes. Diameter = 0.045 m.

S2. ^{1}H Nuclear Magnetic Resonance (^{1}H-NMR) spectra

^{1}H-NMR spectra were acquired on a Bruker AV-300 spectrometer, running at 300 MHz for ^{1}H. Chemical shifts (δ) are reported in ppm relative to the residual solvent signal with a value of 2.50 ppm for DMSO-d_6. The samples were prepared by digestion (100 µL D_2O, 50 µL hydrofluoric acid, and 500 µL DMSO-d_6) of as-synthesized sample MOF-808 NPs and Cu-MOF-808 NPs.

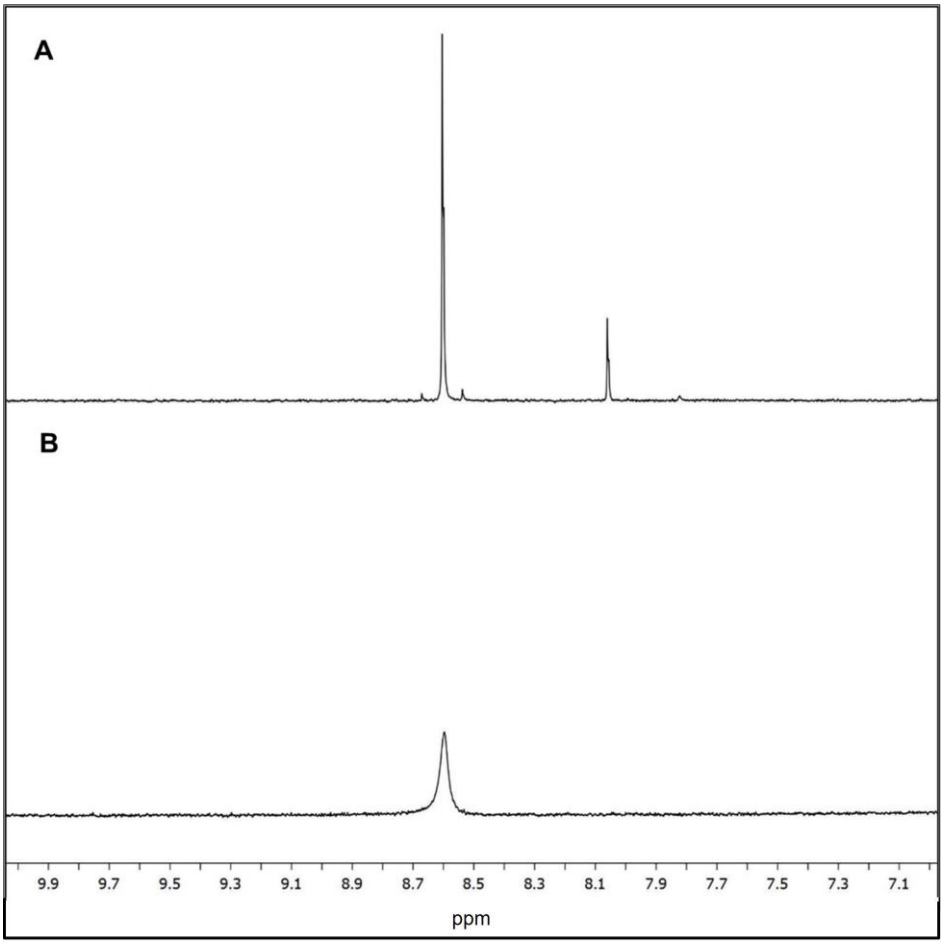

Figure S2.1. Aromatic region of the ^{1}H NMR spectra obtained for (A) MOF-808 NPs and (B) Cu-MOF-808 NPs in DMSO-d_6 after digestion, at 300 MHz.

S3. Transmission Electron Microscopy (TEM). Energy Dispersing X-ray Spectroscopy (EDS)

TEM images were collected on a JEOL JEM 1400 equipment with a power of 120 kV. The samples were prepared by dispersing the materials in ethanol.

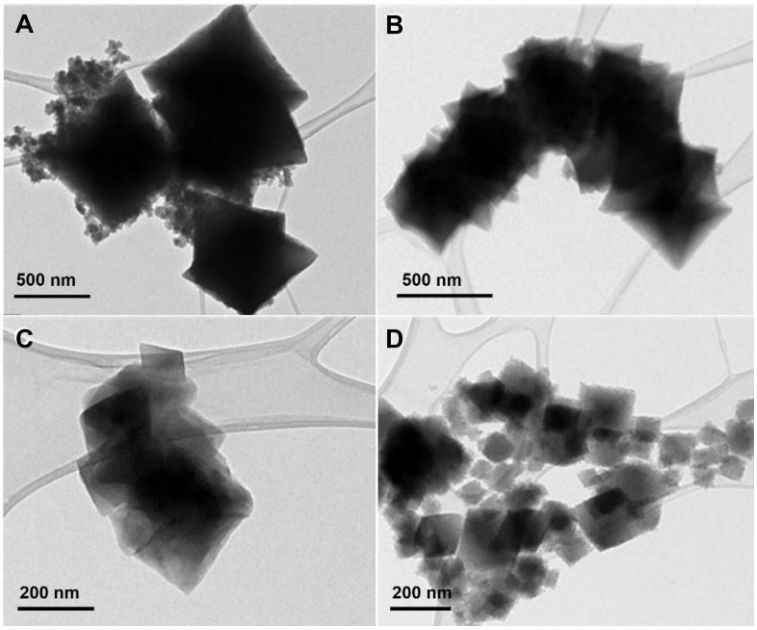

Figure S3.1. TEM images for MOF-808 NPs obtained at (A) 30, (B) 60, (C) 75, and (D) 90 minutes of reaction times.

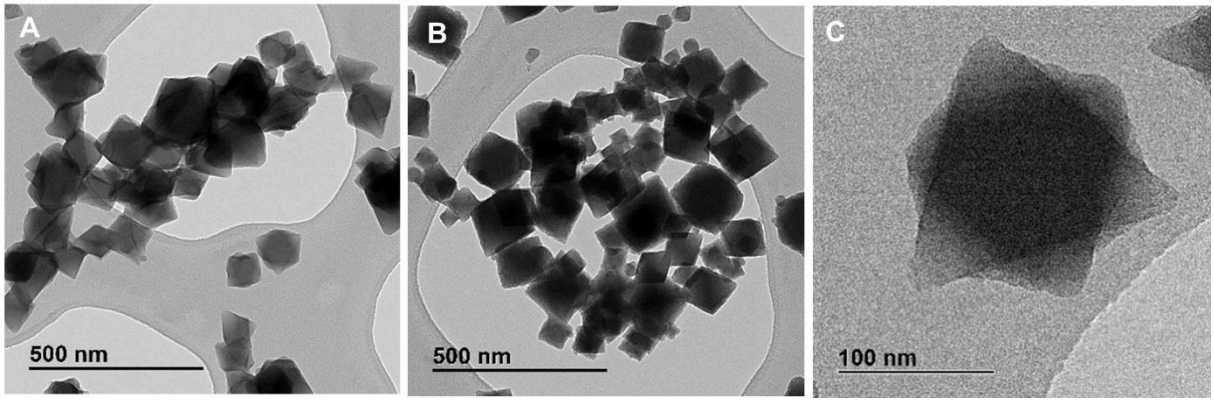

Figure S3.2. TEM images for (A) MOF-808 NPs obtained at 45 minutes, (B) Cu-MOF-808 NPs, and (C) crystal of Cu-MOF-808.

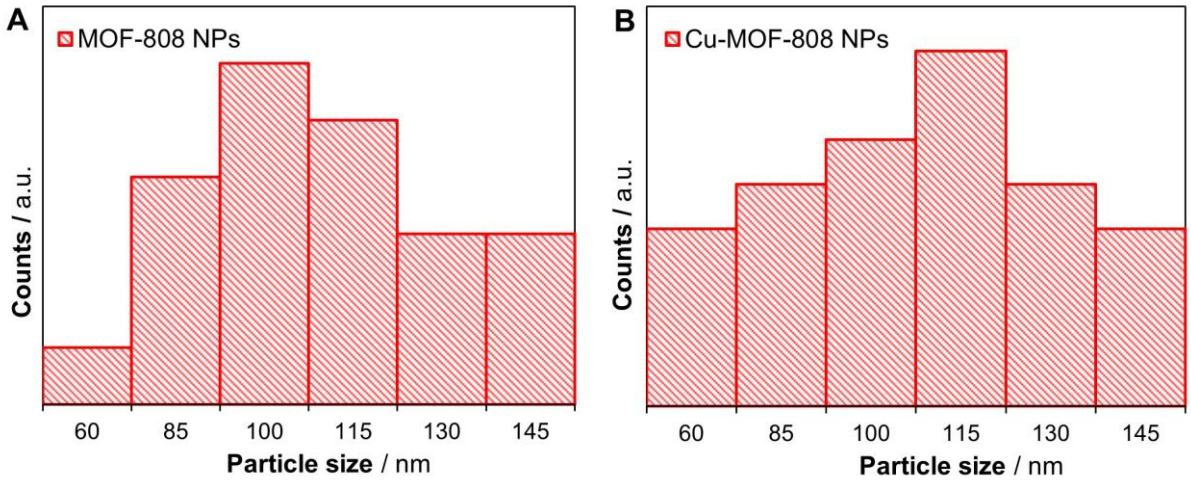

Figure S3.3. (A) Histogram of particle size of MOF-808 NPs obtained at 45 minutes of reaction time. (B) Histogram for Cu-MOF-808 NPs.

S4. Field-Emission Scanning Electron Microscopy (FE-SEM)

FE-SEM images were collected with an FEI VERIOS 460 microscope with a resolution of 0.6 nm at 2 kV and 0.7 nm at 1 kV. The samples were dispersed using dichloromethane and then coated with Au.

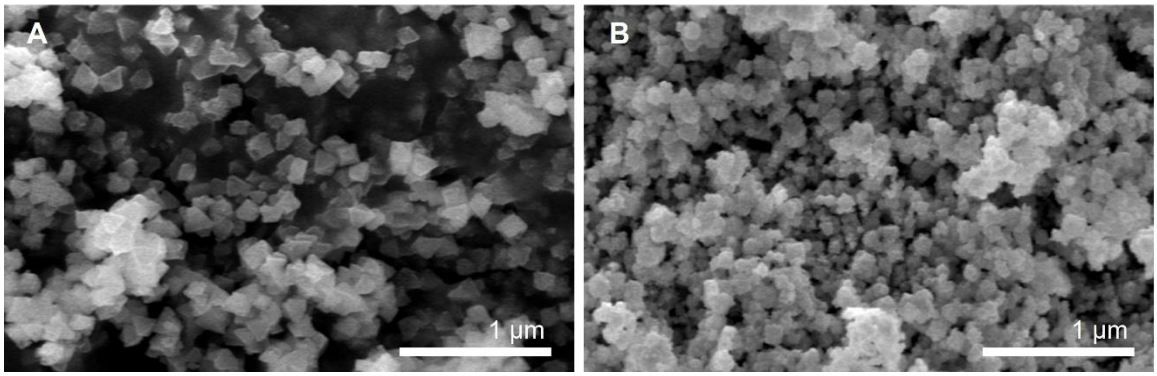

Figure S4.1. FE-SEM images for MOF-808 NPs obtained at (A) 45 and (B) 90 minutes of reaction times.

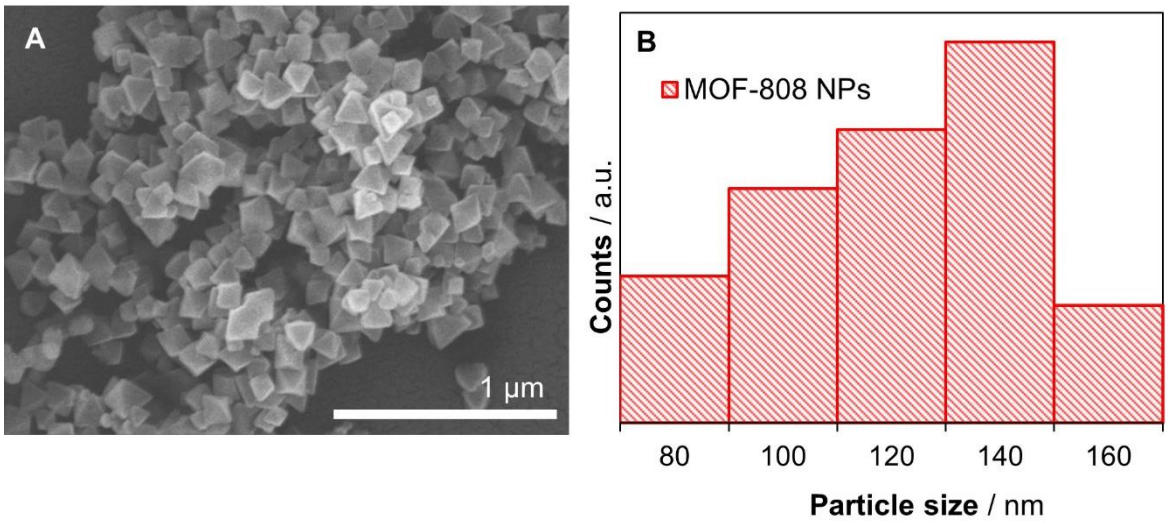

Figure S4.2. (A) FE-SEM image and (B) histogram of MOF-808 NPs obtained at 45 minutes of reaction time.

S5. Scanning Electron Microscopy (SEM). Energy Dispersing X-ray Spectroscopy (EDS)

SEM images were collected with a HITACHI S-3000N microscope equipped with EDX analyzer Quantax EDS. All samples were previously metalated with Au. For the cross-sectional images, membranes were prepared by fracturing them in liquid nitrogen.

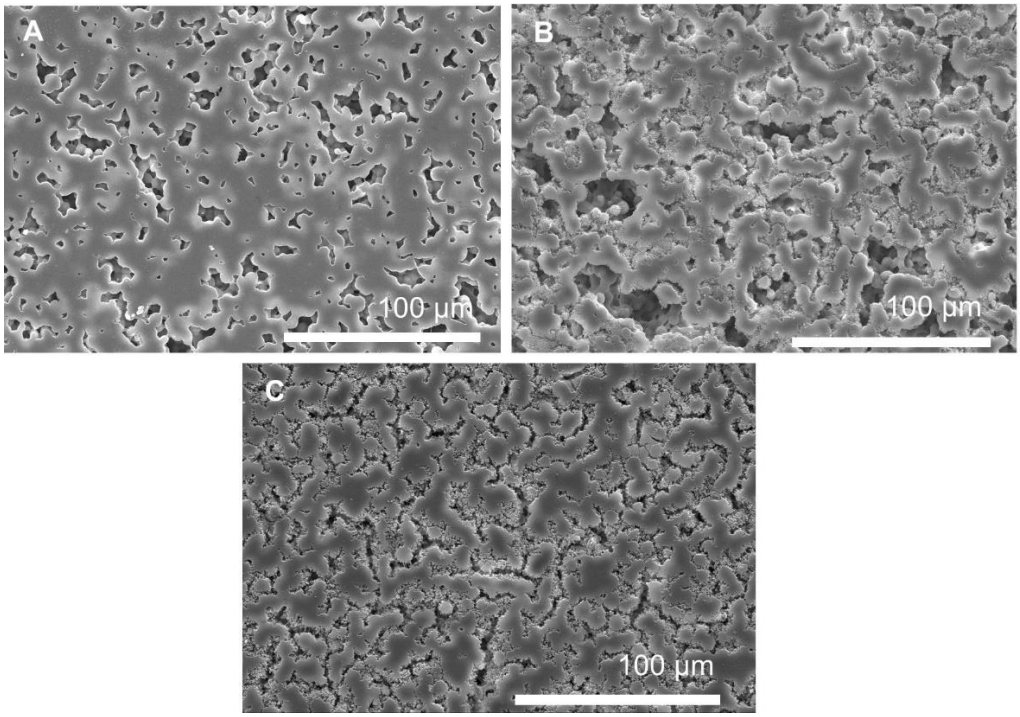

Figure S5.1. SEM accumulating images of the surface of (A) PVDF, (B) MOF-808@PVDF, and (C) Cu-MOF-808@PVDF membranes.

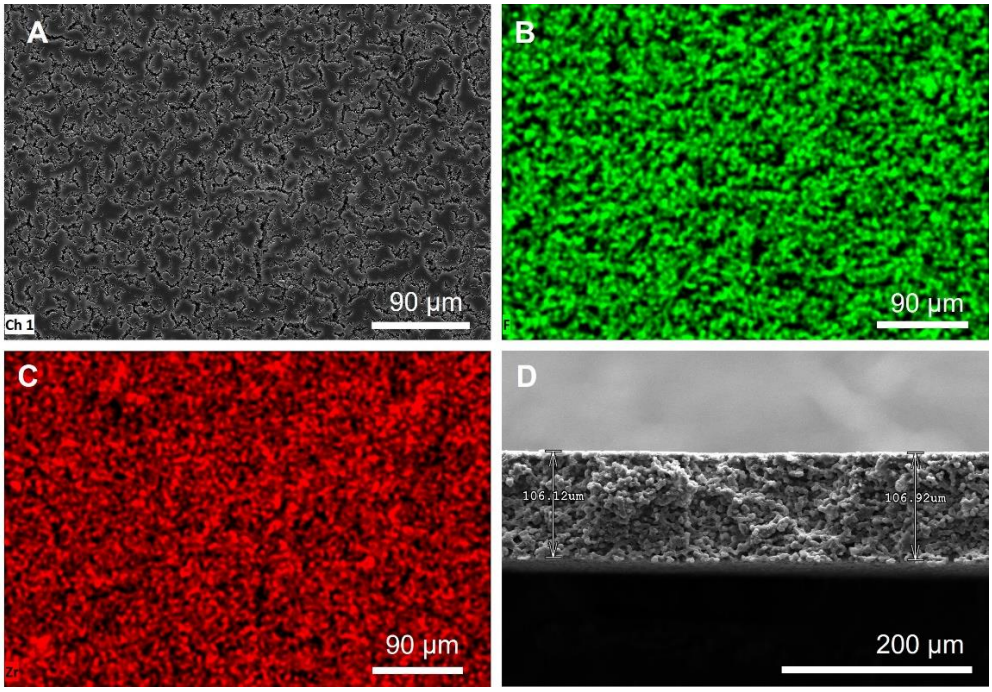

Figure S5.2. SEM-EDS elemental mapping of (A) MOF-808@PVDF MMM, (B) F (green), and (C) Zr (red). (D) SEM cross-section image of MOF-808@PVDF MMM with the thickness of the membrane measured.

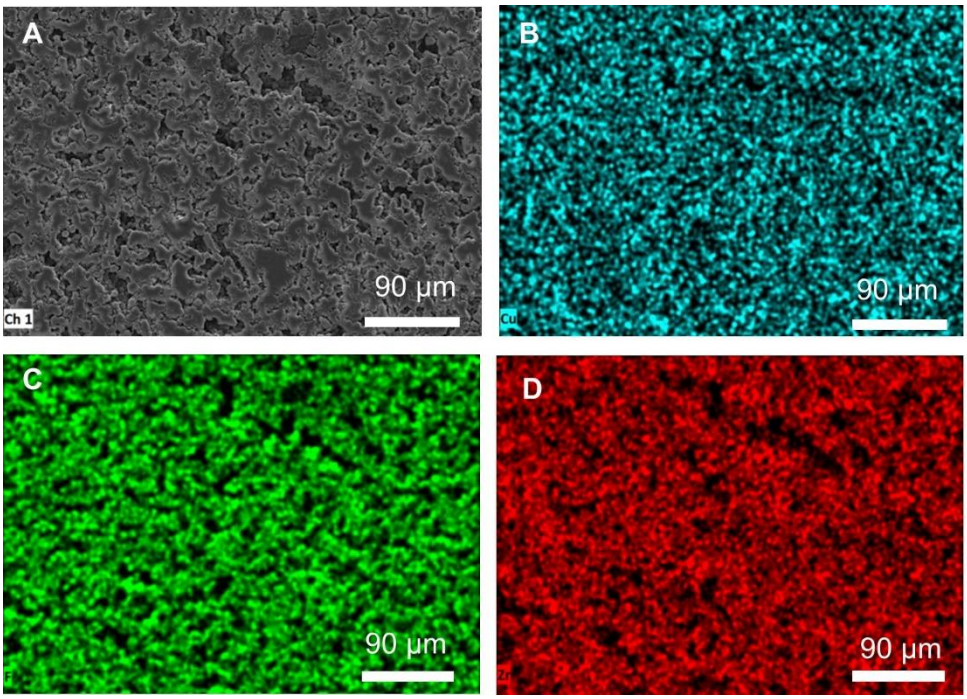

Figure S5.3. SEM-EDS elemental mapping of (A) Cu-MOF-808@PVDF MMM, (B) Cu (blue), (C) F (green), and (D) Zr (red).

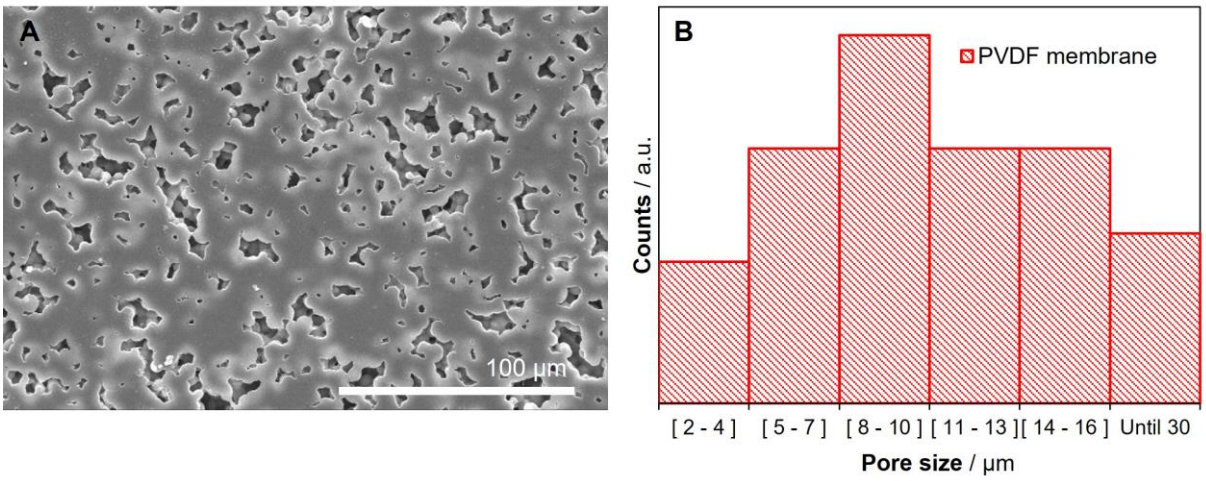

Figure S5.4. (A) SEM image of the PVDF membrane. (B) Histogram of the pore size of the PVDF membrane.

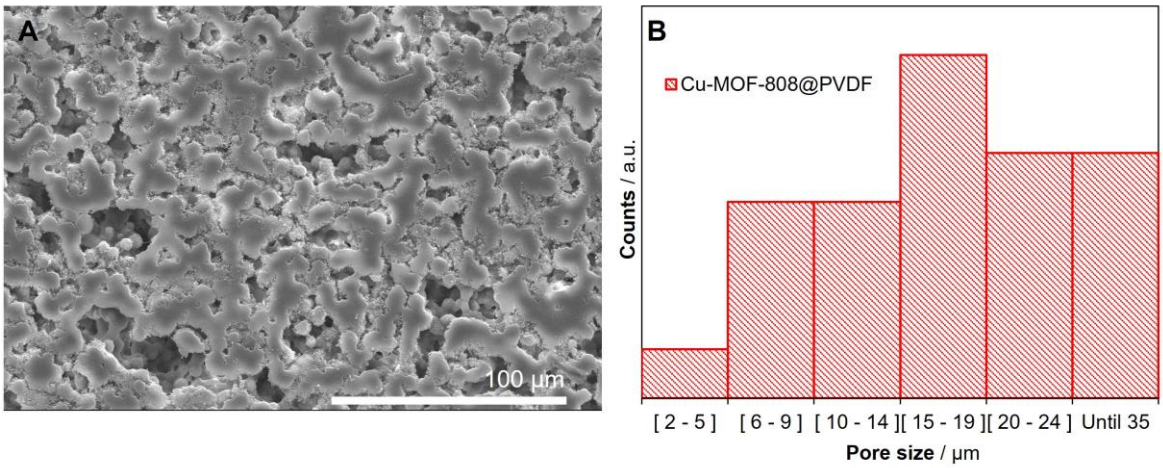

Figure S5.5. (A) SEM image of the Cu-MOF-808@PVDF membrane. (B) Histogram of the pore size of Cu-MOF-808@PVDF.

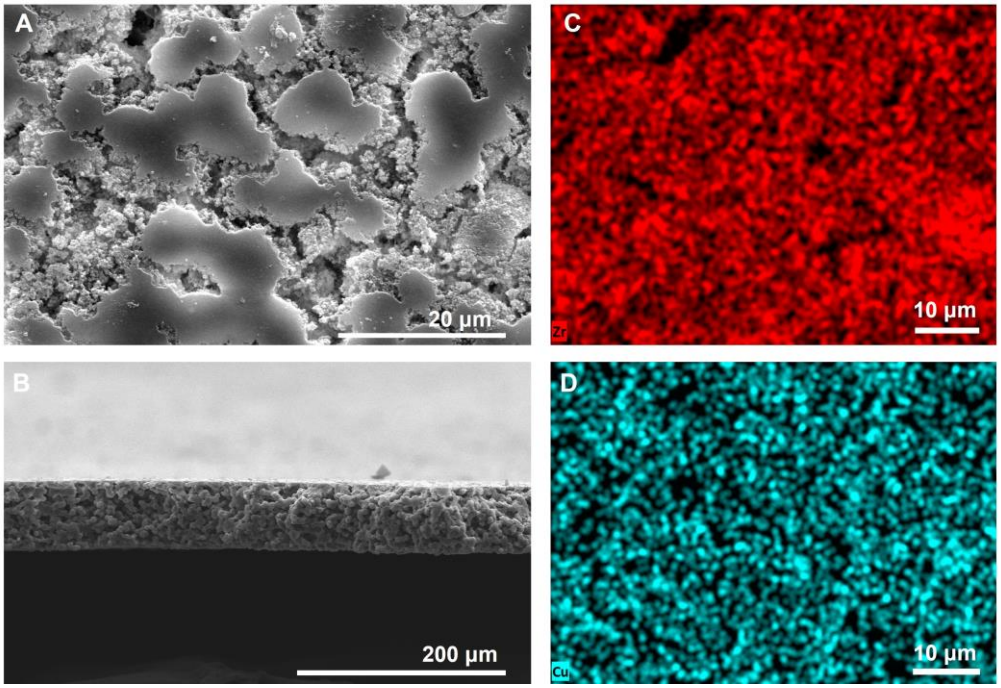

Figure S5.6. SEM-EDS elemental mapping of (A) Cu-MOF-808@PVDF MMM surface after 8 months (B) Cu-MOF-808@PVDF MMM cross section after 8 months. Elemental mapping (C) Zr (red) and (D) Cu (blue). For the assessment of the long-term stability of the membranes.

S6. Dynamic Light Scattering (DLS)

Particle size measurements based on DLS were performed in a VASCO nanoparticle size analyzer from Cordouan Technologies, designed for nanoparticle suspension and colloidal characterization in suspension. Analyses were carried out at 25 ºC, taking 100 acquisitions and using Pade Laplace and Cumulants as algorithms. Samples were prepared by sonicating a mixture of 2 mg MOF in 10 mL solvent (DMF) for 30 min.

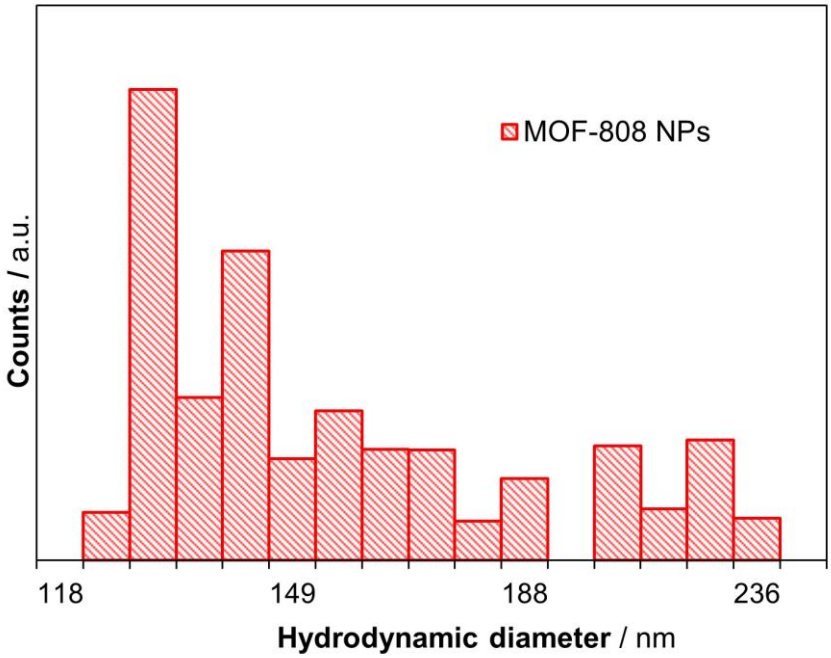

Figure S6.1. DLS histogram obtained for MOF-808 NPs suspended in DMF.

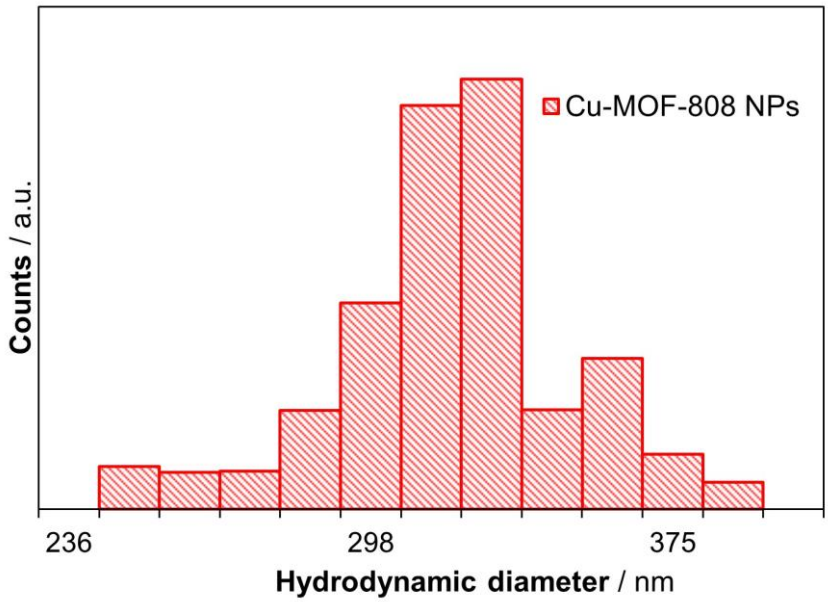

Figure S6.2. DLS histogram obtained for Cu-MOF-808 NPs suspended in DMF.

S7. Powder X-ray Diffraction (PXRD)

PXRD data were collected with a Bruker D8 diffractometer equipped with a copper source operated at 1600 W, with step size = 0.02 ° and exposure time = 0.50 s/step. Samples were placed on a borosilicate sample holder and then the sample surface was leveled with a clean microscope slide. All the samples were ground before analysis unless otherwise stated. For the membranes, PXRD data were measured in the transmission method. Data were measured using a continuous 2θ scan from 3.0 º to 45.0 º.

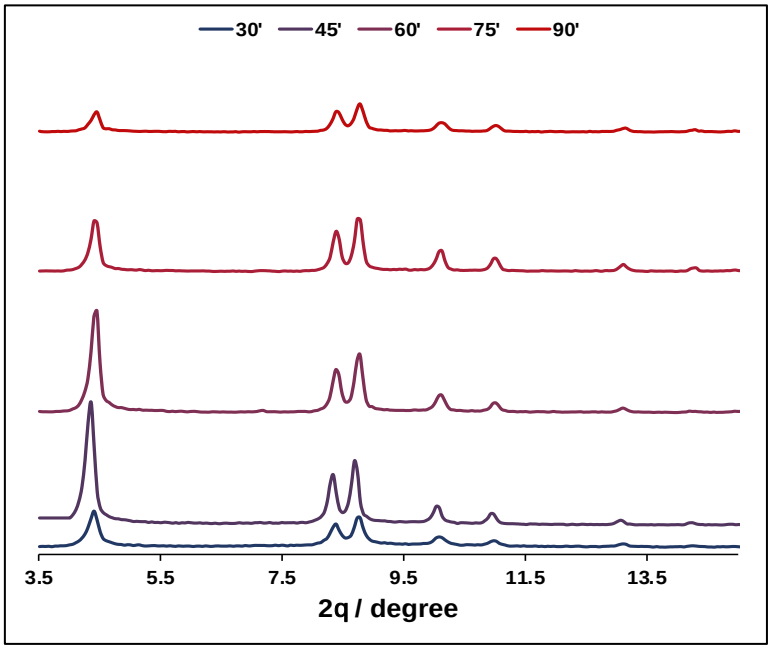

Figure S7.1. PXRD data for MOF-808 NPs obtained at different microwave-assisted reaction conditions.

PXRD data of the Cu-MOF-808 NPs show a high crystallinity and pure phases compared with the calculated pattern from single crystal data (Figure S7.2).[1] A slight loss of crystallinity is observed in the materials after catalysts due to the oxidant conditions employed.

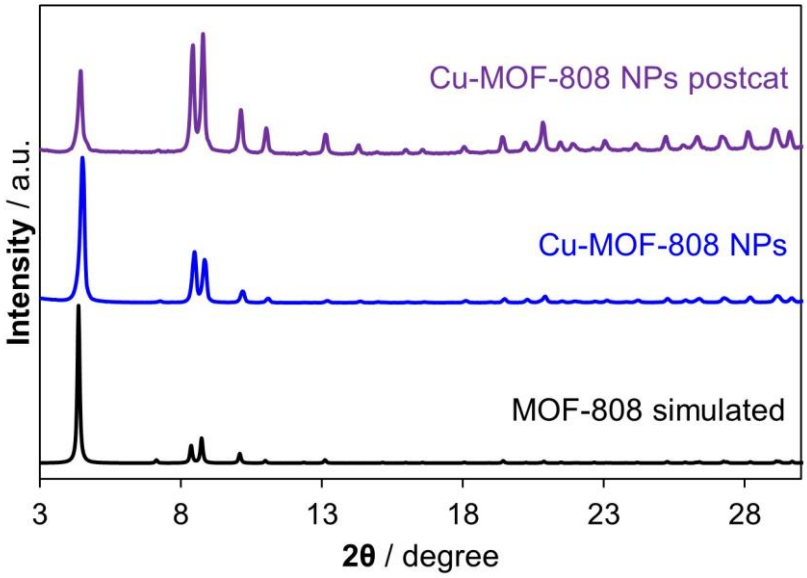

Figure S7.2. PXRD data of the Cu-MOF-808 NPs before and after catalysis.

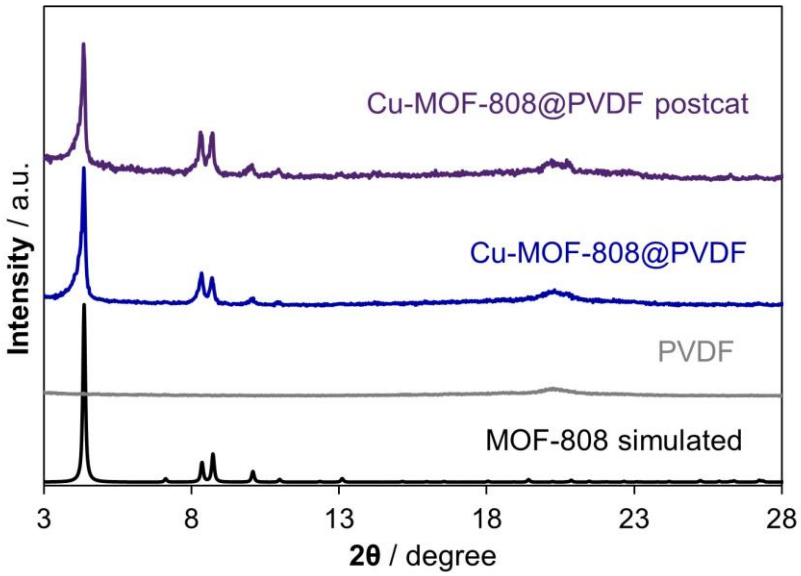

Figure S7.3. PXRD data of the membranes before and after catalysis.

Table S7.1. Pawley refinement values for the hybrid membrane.

Sample	*Lattice / Å*	*Rwp / %*	*Rp / %*
Cu-MOF-808@PVDF	35.29	14	12

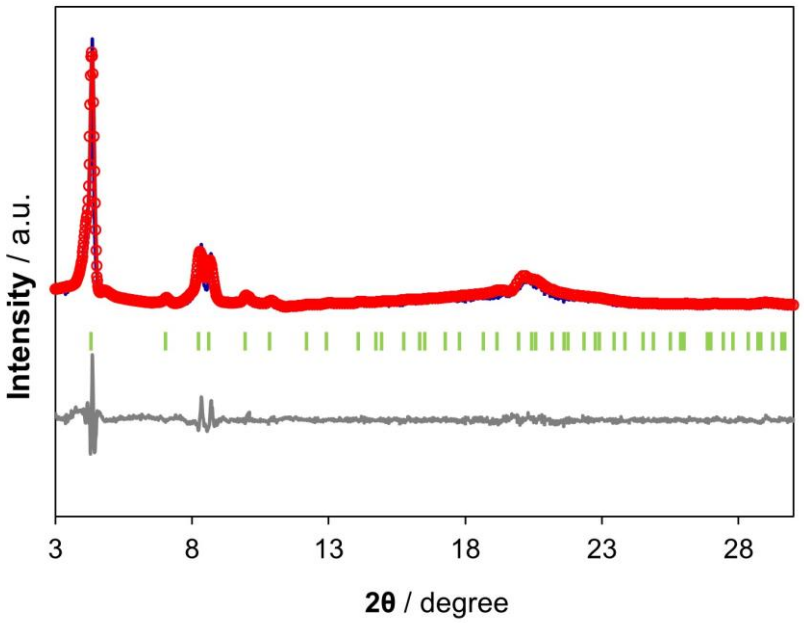

Figure S7.4. Pawley refinement for Cu-MOF-808@PVDF. Calculated (red), experimental (blue), difference (grey), and Bragg positions (green).

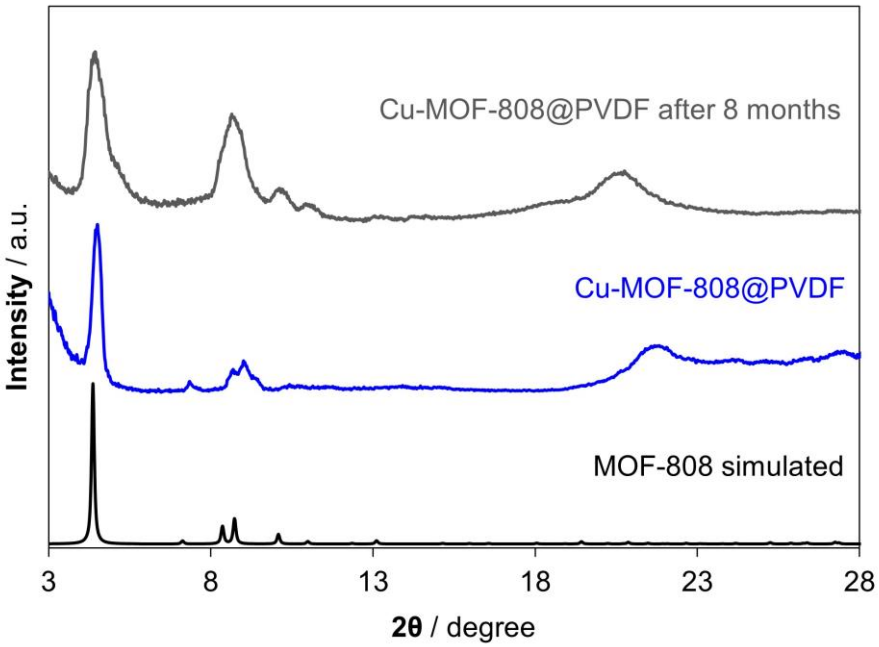

Figure S7.5. PXRD data (in reflection mode) of the membrane after 8 months for the assessment of the long-term stability of the membranes.

S8. Attenuated total reflectance (ATR) for Fourier-transform infrared spectroscopy (FTIR)

ATR-FTIR analyses were recorded on a PerkinElmer 100 spectrophotometer using a PIKE Technologies MIRacle Single Reflection Horizontal ATR Accessory from 4000-450 cm^{-1}.

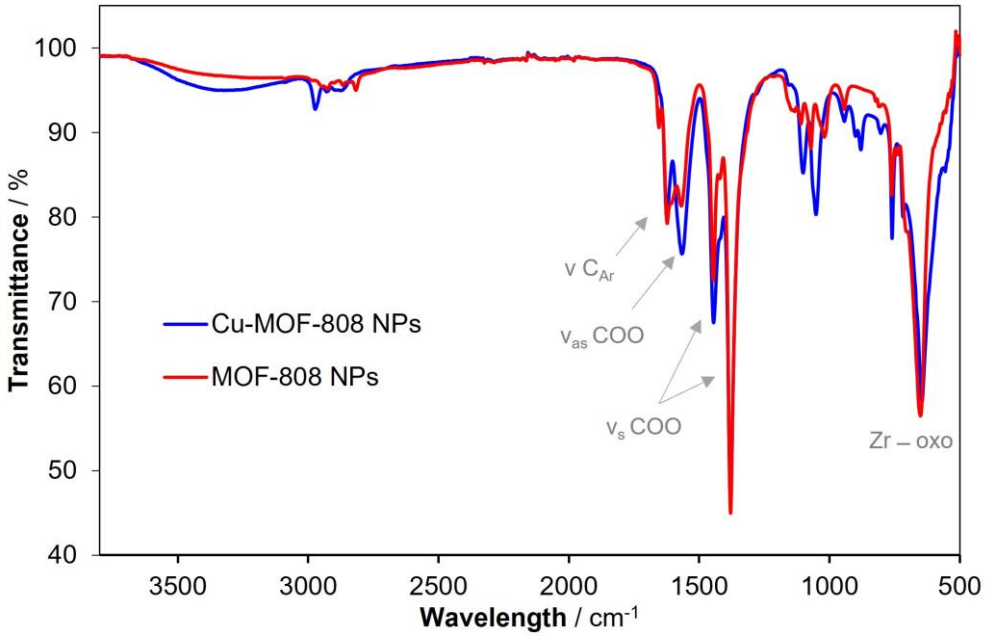

Figure S8.1. ATR-FTIR spectra of MOF-808 and Cu-MOF-808 NPs.

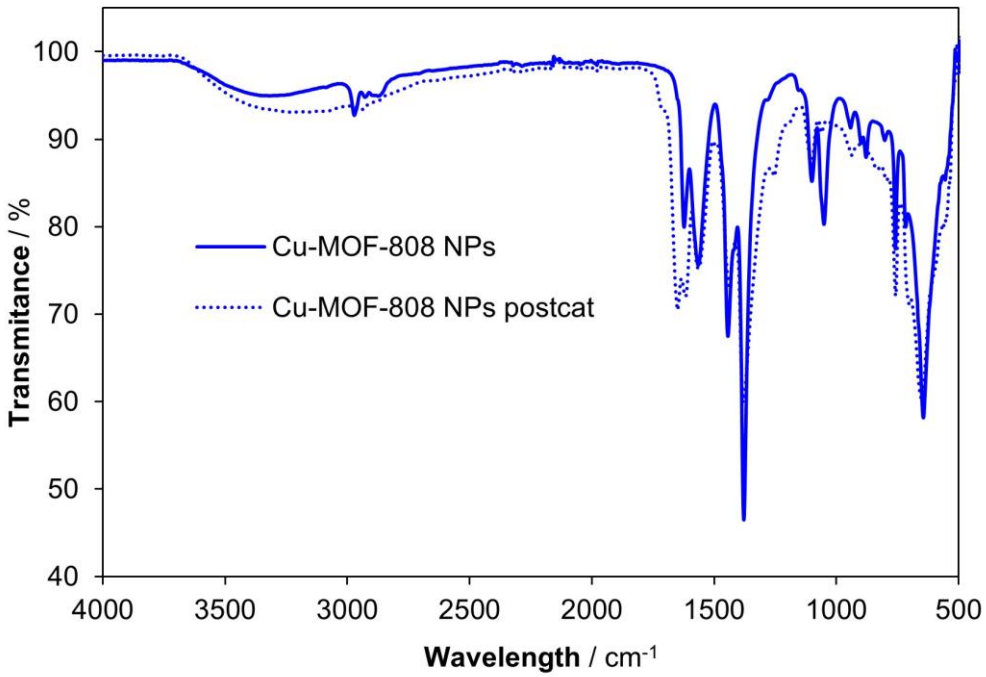

Figure S8.2. ATR-FTIR spectra of Cu-MOF-808 NPs before and after catalysis.

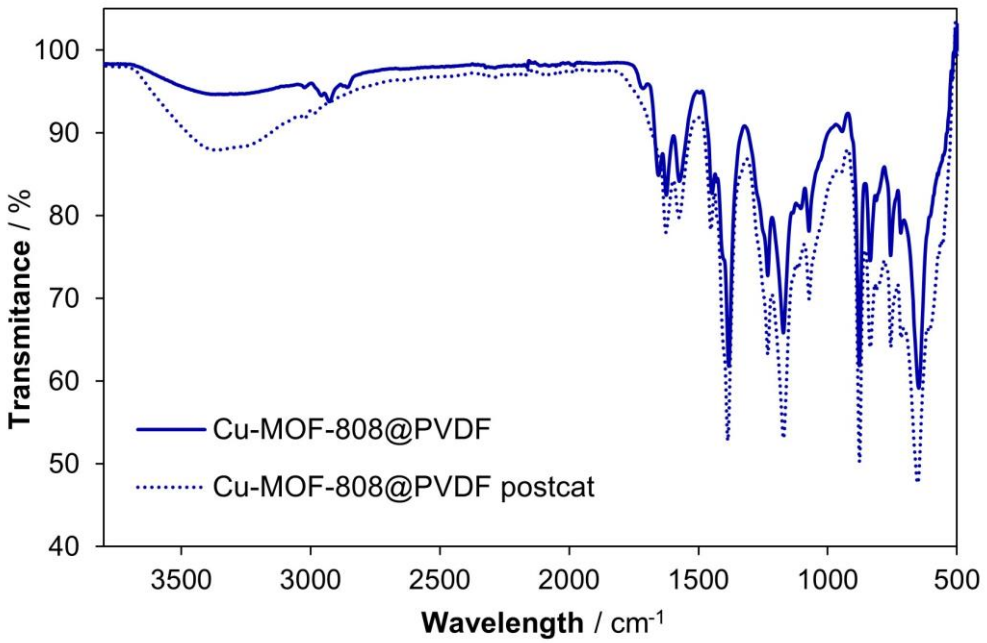

Figure S8.3. ATR-FTIR spectra of the Cu-MOF-808@PVDF membrane before and after catalysis.

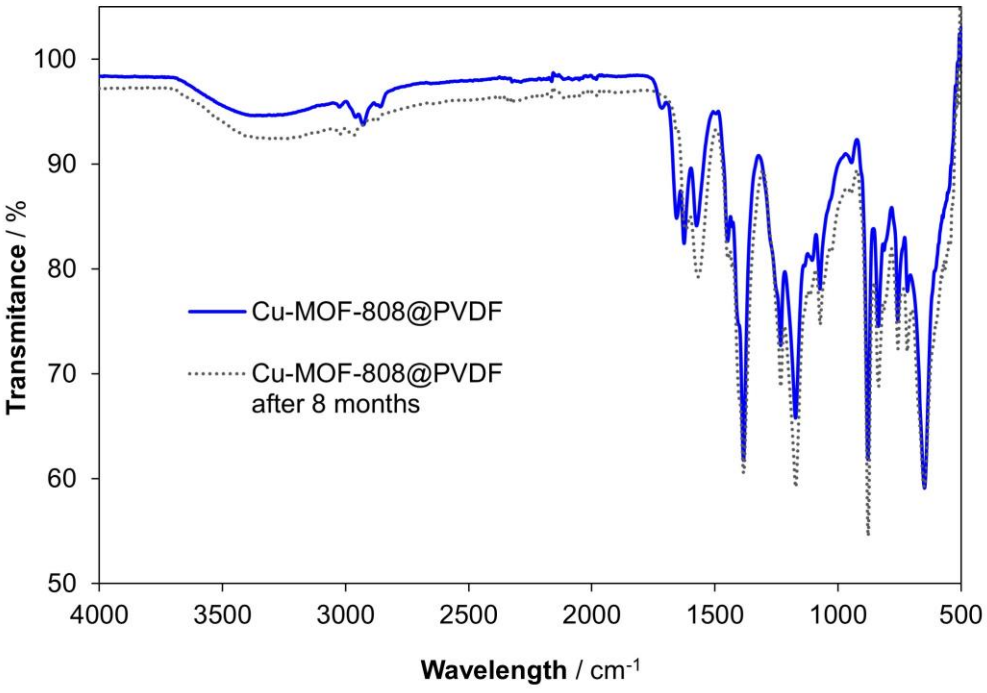

Figure S8.4. ATR-FTIR spectra of the Cu-MOF-808@PVDF membrane after 8 months for the assessment of the long-term stability of the membranes.

S9. Thermogravimetric analysis and differential thermal analyses (TGA-DTA)

TGA-DTA were performed using an SDT Q600 from TA Instruments equipment in a temperature range between 20 °C and 800 °C in the air (100 mL·min^{-1} flow) atmosphere and heating rate of 10 ºC·min^{-1}.

For the MOF-808 NPs (Figure S9.1), there is a mass loss associated with the water molecules with a value of 17.40 %. In the temperature range of 200-600 ºC, there is a 38.35 % weight loss corresponding to the decomposition of BTC ligands, formates, and DMF left (calculated at 33.30 %). All weight loss from 20 ºC to 800 ºC is 55.75 % which matches the conversion of MOF-808 NPs to the residual of this material, ZrO_2 (62.3 % calculated).

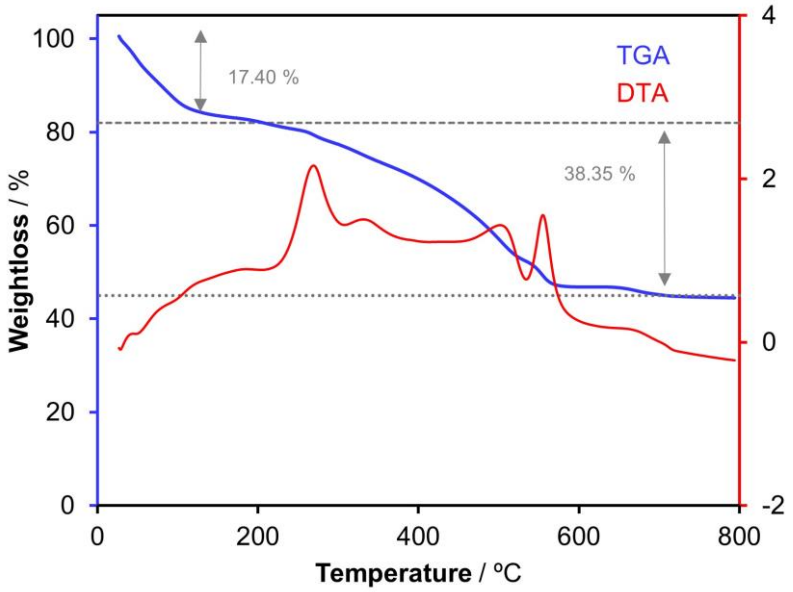

Figure S9.1. TGA and DTA of MOF-808 NPs.

For the Cu-MOF-808 NPs (Figure S9.2) there is a mass loss associated with the water molecules with a value of 16.59 %. In the temperature range of 200-600 ºC, there is a 26.62 % weight loss corresponding to the decomposition of BTC ligands (calculated at 26.80 %). The weight loss from 20 ºC to 800 ºC is 52.18 % which matches the conversion of Cu-MOF-808 to the residues of this material, ZrO_2 and CuO (55.10 % calculated).

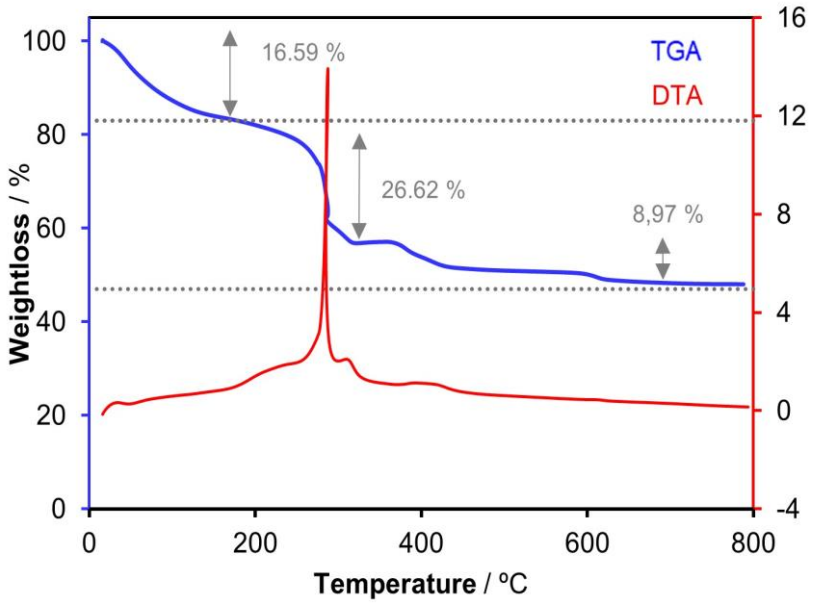

Figure S9.2. TGA and DTA of Cu-MOF-808 NPs.

TGA data collected on all the membranes showed a mass loss associated with the loss of the polymeric organic. For the membranes with MOF, we can observe that the combustion was not total, the residue of 6.00 wt% corresponds to the inorganic salts formed by the metals Zr and Cu (Figure S9.3, Figure S9.4, and Figure S9.5).

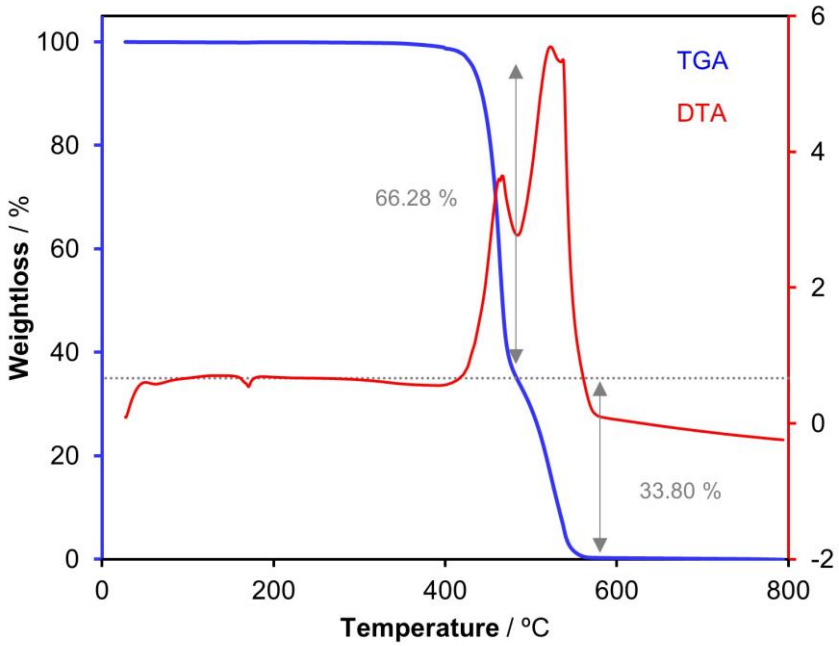

Figure S9.3. TGA and DTA of PVDF.

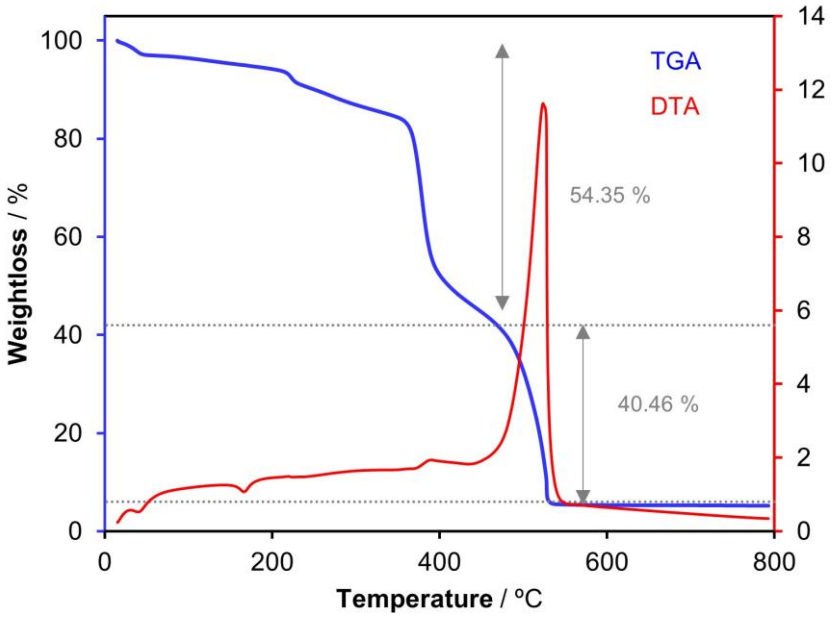

Figure S9.4. TGA and DTA of MOF-808@PVDF.

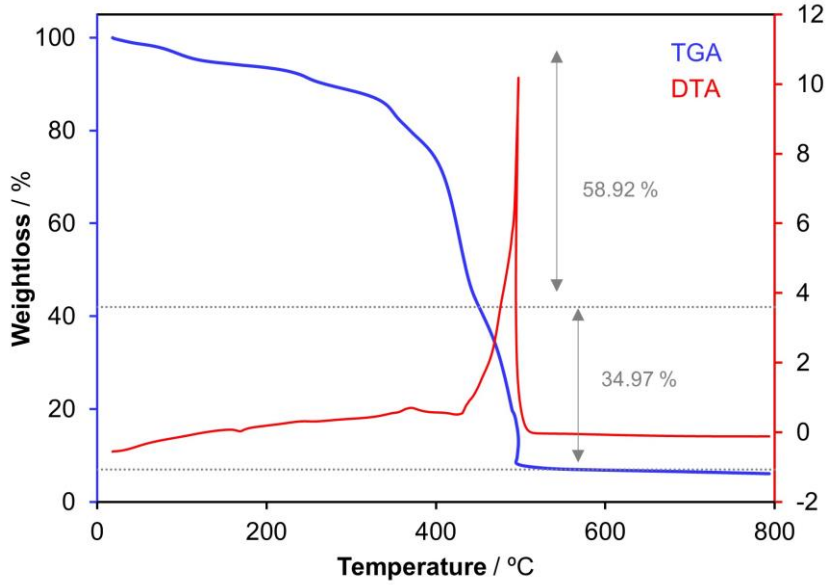

Figure S9.5. TGA and DTA of PVDF Cu-MOF-808@MMM.

S10. Textural analyses: Nitrogen adsorption isotherms

Nitrogen adsorption and desorption isotherms were measured at 77 K using a Micromeritics ASAP 2020 system. The samples were outgassed at 150 ºC for 16 h before the measurements. The specific surface areas (BET) were calculated by applying the Brunauer-Emmett-Teller equation, taking the nitrogen molecule's area as 0.16 nm^2. The BET equation's linear range was between 0.05 and 0.35 P/P_0. However, for all other materials studied due to their microporous natures, this linear range was much narrower and displaced to lower relative pressures: P/P_0= 0.04–0.07. The micropore volume and the external surface area, *i.e.* the area not associated with the micropores, were calculated using a t-plot analysis. The total pore volume was calculated from the volume of gas adsorbed at a relative pressure of 0.95 on the adsorption branch of the isotherms. The pore-size-distribution (PSD) curves were obtained from the adsorption branches using the non-local density functional theory (NLDFT) method for a cylinder pore in pillared clays, using regularization of 0.10.

Table S10.1. Data collected from N_2 isotherms at 77K, BET, and t-plot analysis.

Sample	*S_{BET} / m^2g^{-1}*	*External area / m^2g^{-1}*	*Micropore volume / cm^3g^{-1}*	*Total pore volume / cm^3g^{-1}*
MOF-808 NPs	2035.67	88.24	0.73	1.12
Cu-MOF-808 NPs	1370.82	107.22	0.47	0.68

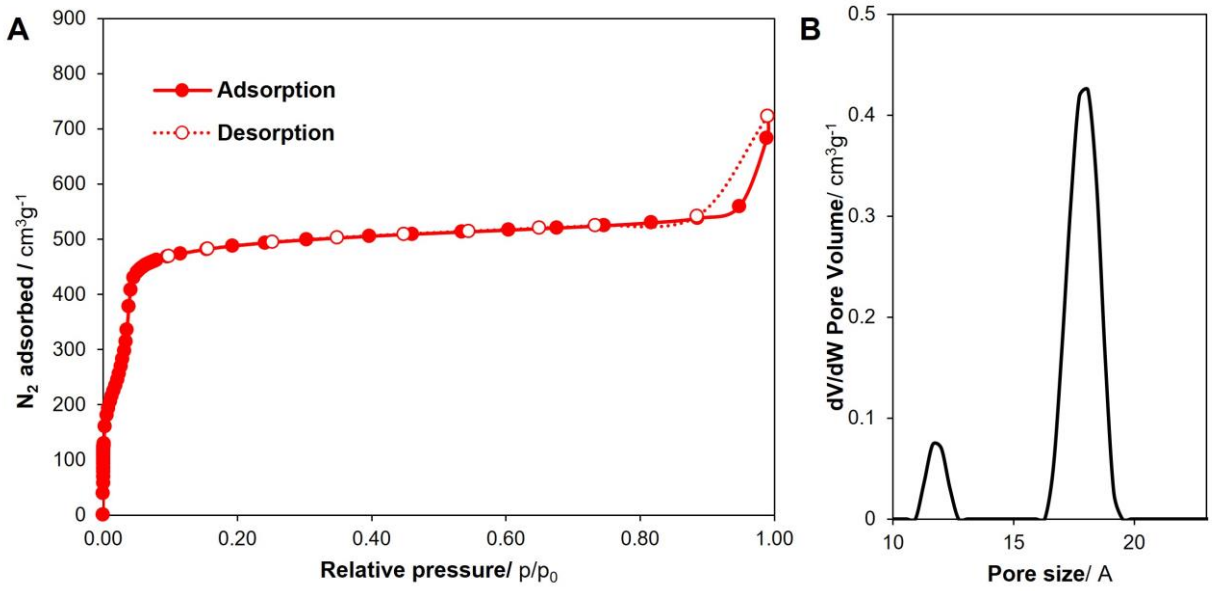

Figure S10.1. (A) N_2 adsorption isotherms and (B) NLDFT pore size distribution for MOF-808 NPs.

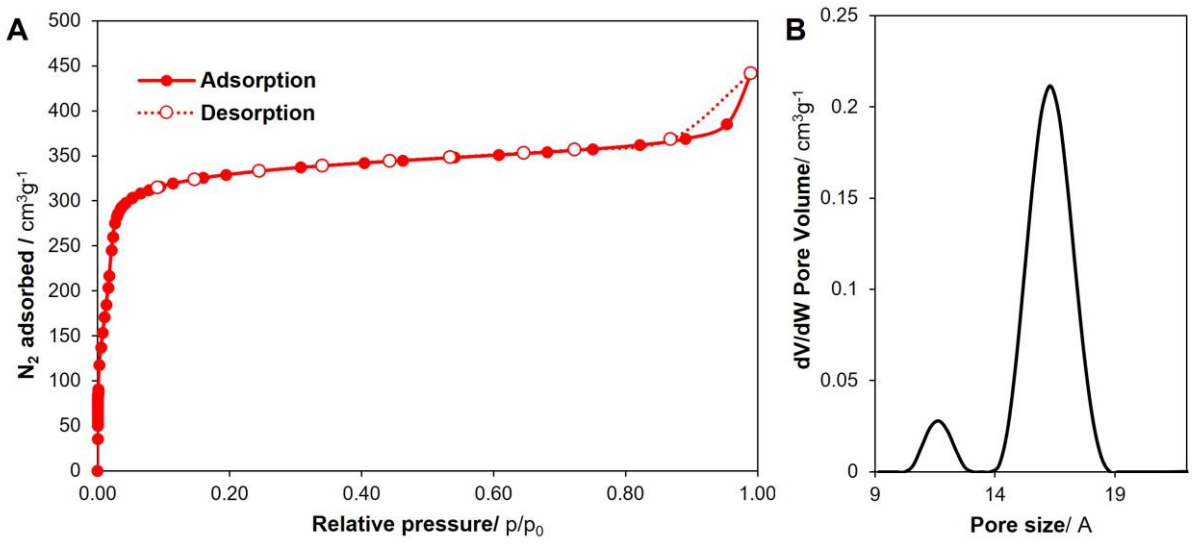

Figure S10.2. (A) N_2 adsorption isotherms and (B) NLDFT pore size distribution for Cu-MOF-808 NPs.

S11. X-Ray Absorption Spectroscopy (XAS)

Transmission and fluorescence geometry XAS measurements were performed at the BL22-CLAESS beamline at ALBA Synchrotron. Cu K-edge XAS spectra were acquired with a k-range up to 10.5 $Å^{-1}$. The data analysis and background removal were performed within ATHENA and ARTEMIS.[3] CuO was employed as a reference. The data were collected at 20 K. Both X-ray absorption near-edge structure (XANES) and extended X-ray absorption fine structure (EXAFS) data were analyzed.

Characterization of the membrane before and after catalysis where the retainment of the structure of the copper sites and the oxidation state of copper is proven being the spectra of both very similar only showing the presence of copper (II) species. As previously reported by us[2] the quadrupole-allowed 1s/3d transition seen around 8984 eV indicates the presence of Cu(II) in a twisted-square-planar geometry.

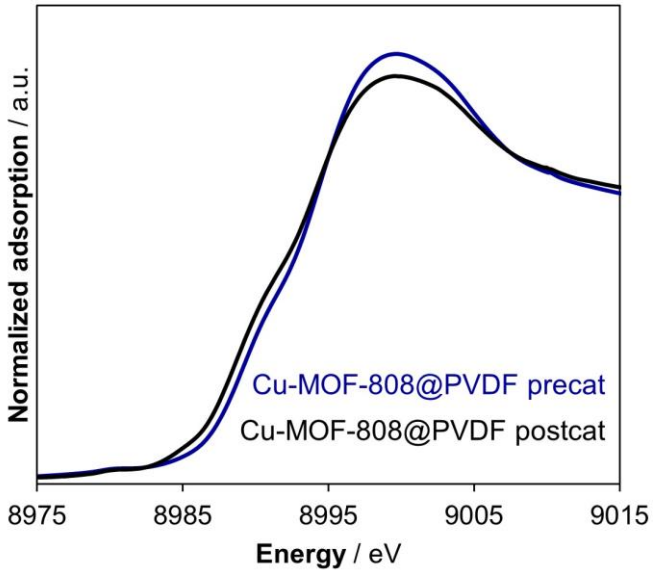

Figure S11.1. XANES data of the Cu-MOF-808@PVDF membranes pre and postcatalysis.

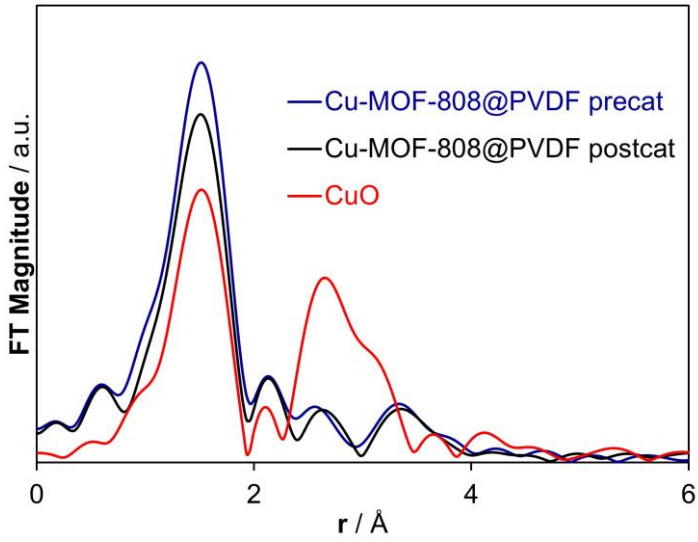

Figure S11.2. EXAFS data of the Cu-MOF-808@PVDF membranes pre and postcatalysis compared with CuO salt.

Table S11.1. Bond distances, coordination numbers, N, Debye-Waller factors, σ^2, and inner potential corrections, ΔE_0, for the EXAFS fit of the Cu-MOF-808@PVDF membrane precatalysis.

Path	Distance, Å	N[a]	σ^2, Å^2	ΔE_0, eV[b]	S_0^2
Cu-O	1.909(8) 1.985(8)	4	0.004(1)	5(1)	1.04(9)
Cu···Zr	3.3(4)	1	0.01(4)		

[a] The coordination numbers, N, were fixed according to the DFT model.[2]

[b] The energy shift is constrained to be equal for all paths.

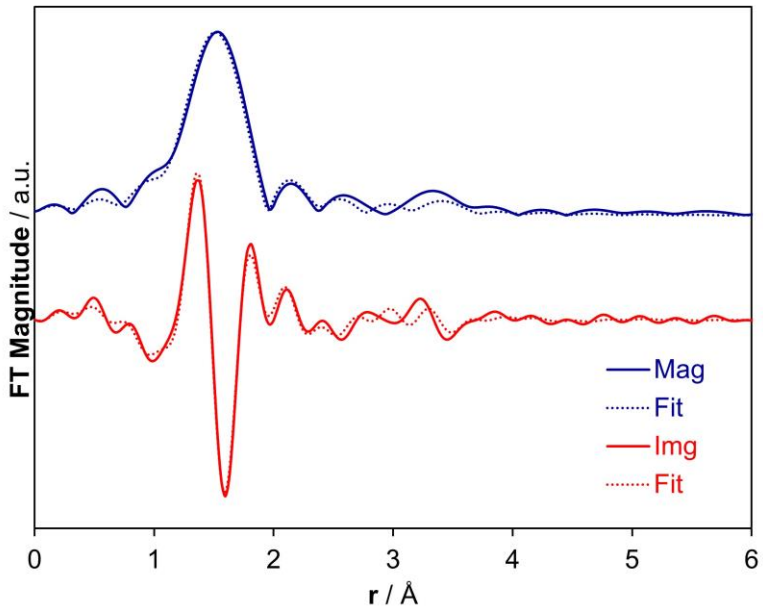

Figure S11.3. EXAFS k^2-weighted Cu K-edge Mag[χ(R)] (solid line) and its respective fit (dash line) together with Img[χ(R)] (solid line) and its fit (dash line) spectra of Cu-MOF-808@PVDF.

Table S11.2. Bond distances, coordination numbers, N, Debye-Waller factors, σ^2, and inner potential corrections, ΔE_0, for the EXAFS fit of the Cu-MOF-808@PVDF membrane postcatalysis.

Path	Distance, Å	N[a]	σ^2, Å^2	ΔE_0, eV[b]	S_0^2
Cu-O	1.91(2) 1.99(2)	4	0.003(1)	4(1)	0.87(9)
Cu···Zr	3.31(7)	1	0.009(4)		

[a] The coordination numbers, N, were fixed according to the DFT model.[2]

[b] The energy shift is constrained to be equal for all paths.

S12. Pair Distribution Function (PDF) analysis

Synchrotron X-ray total scattering data suitable for PDF analysis were collected at the I15-1 beamline at Diamond Synchrotron using 65 keV (0.190 Å) X-rays. Samples were loaded in glass capillaries (1 mm and 2 mm Ø) and sealed by welding. Geometric corrections and reduction to 1D data used DAWN Science software.[4] PDFs patterns were obtained from the data within PDFgetX3 within xPDFsuite to a Q_{max} = 19 $Å^{-1}$.[5] Differential PDFs were obtained by subtraction of PDF profiles in real space after applying a normalization factor.

To assess the local structure of the copper single sites within the nanoparticles of MOF-808, the differential PDF analysis between them was carried out (Fig.S12.1) obtaining distances in agreement with our previous work.[2]

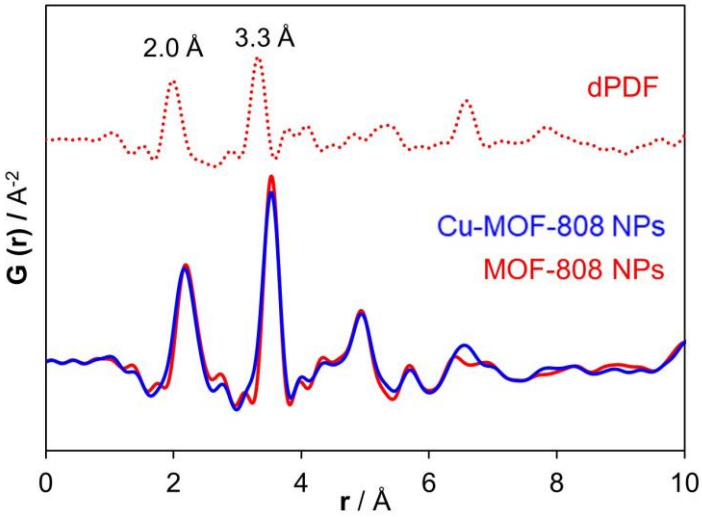

Figure S12.1. dPDF data, revealing the copper single sites, (up) were obtained after subtracting the total PDF data of pristine MOF-808 NPs to that of Cu-MOF-808 NPs (down).

To assess the local structure of the MOF within the membrane, subsequent differential analysis was carried out (Figure S12.2).

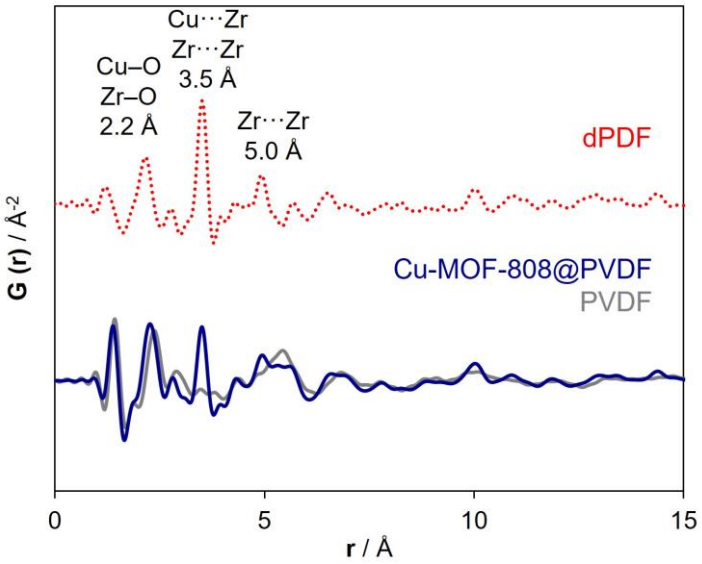

Figure S12.2. dPDF data, revealing the Cu-MOF-808 NPs structure, (up) were obtained after subtracting the total PDF data of PVDF from that of Cu-MOF-808@PVDF (down).

To study the local structure of the copper single sites within the membrane after the catalysis, a differential analysis was performed by subtracting the PDF of MOF-808@PVDF to that of Cu-MOF-808@PVDF postcatalysis (Figure S12.3).

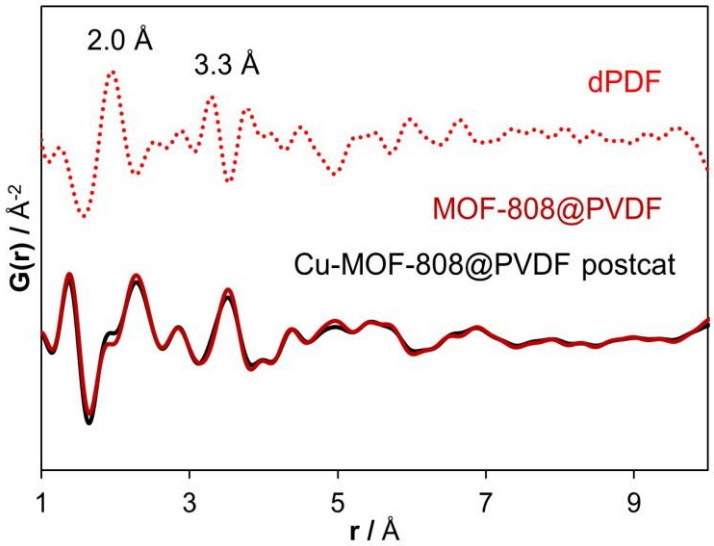

Figure S12.3. dPDF data, revealing the copper single sites after catalysis, (up) were obtained after subtracting the total PDF data of MOF-808@PVDF from that of Cu-MOF-808@PVDF after 8h of reaction (down).

To study the interactions between the pristine MOF-808 and the matrix of the membrane, a PDF differential analysis was carried out highlighting the occurrence of hydrogen bonding between the two phases (Figure S12.4).

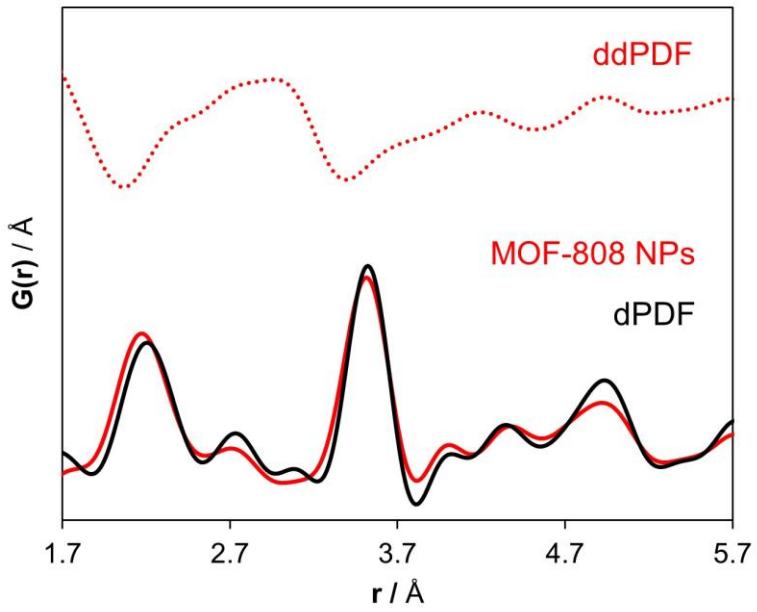

Figure S12.4. ddPDF data, revealing the interactions between MMM and MOF, (up) were obtained after subtracting the total PDF data of MOF-808 NPs from the dPDF obtained from comparing MOF-808@PVDF with PVDF (down).

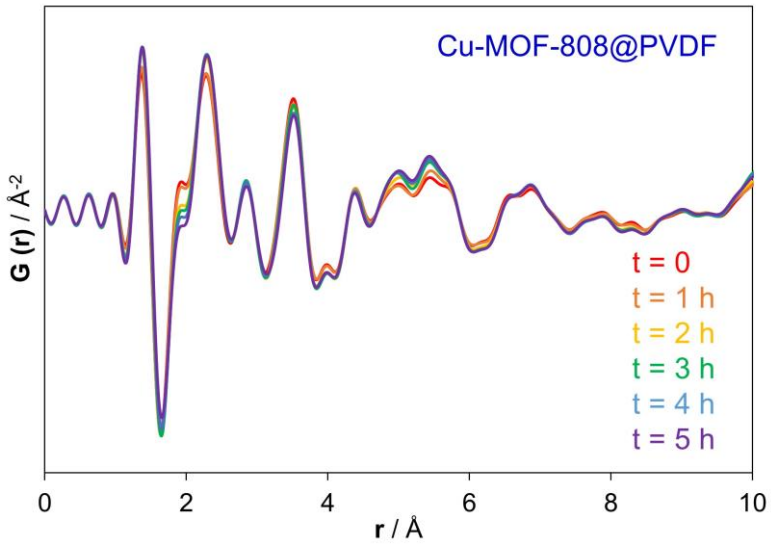

Figure S12.5. PDF patterns obtained for the Cu-MOF-808@PVDF membranes at different times of the catalysis, representing a kinetic study.

S13. Catalytic tests

It has been noted that the initial step involved the uptake of tyrosol using both the prepared powders and membranes under the same conditions as the catalysis experiments. However, the results obtained were insignificant.

Tyrosol (TyrOH) degradation in water through Fenton reactions. Advanced oxidation processes, such as Fenton reactions, are successfully used for the removal of organic pollutants in water. The Fenton reaction is a catalytic process for the generation of hydroxyl radicals, based on electron transfer between hydrogen peroxide and a metal ion. [6] In addition, the reaction shown in equation 0 is another redox process that also takes place and causes the increase of the pH. So, the proposed mechanism for copper species is shown in equations 1 and 2 as previously reported.[7]

$$2Cu^{2+} + H_2O_2 \rightarrow 2H^+ + O_2 + 2Cu^+ \quad (0)$$

$$Cu^{2+} + H_2O_2 \rightarrow Cu^+ + HO_2^{\bullet} + OH^- \ (k = 4.6 \times 102\ M^{-1}{\cdot}s^{-1}) \quad (1)$$

$$Cu^+ + H_2O_2 \rightarrow Cu^{2+} + HO^{\bullet} + HO^- \ (k = 1.0 \times 104\ M^{-1}{\cdot}s^{-1}) \quad (2)$$

The complete reaction with TyrOH ($C_8H_{10}O_2$) is the one shown in equation 3 and the proposed mechanism (Scheme S13.1) was obtained from the literature.[8,9]

$$C_8H_{10}O_2 + {}^{\bullet}OH \rightarrow CO_2 + H_2O \quad (3)$$

Scheme S13.1. The mechanism for the degradation of tyrosol, each narrow indicates a reaction with $HO^{\bullet}$.

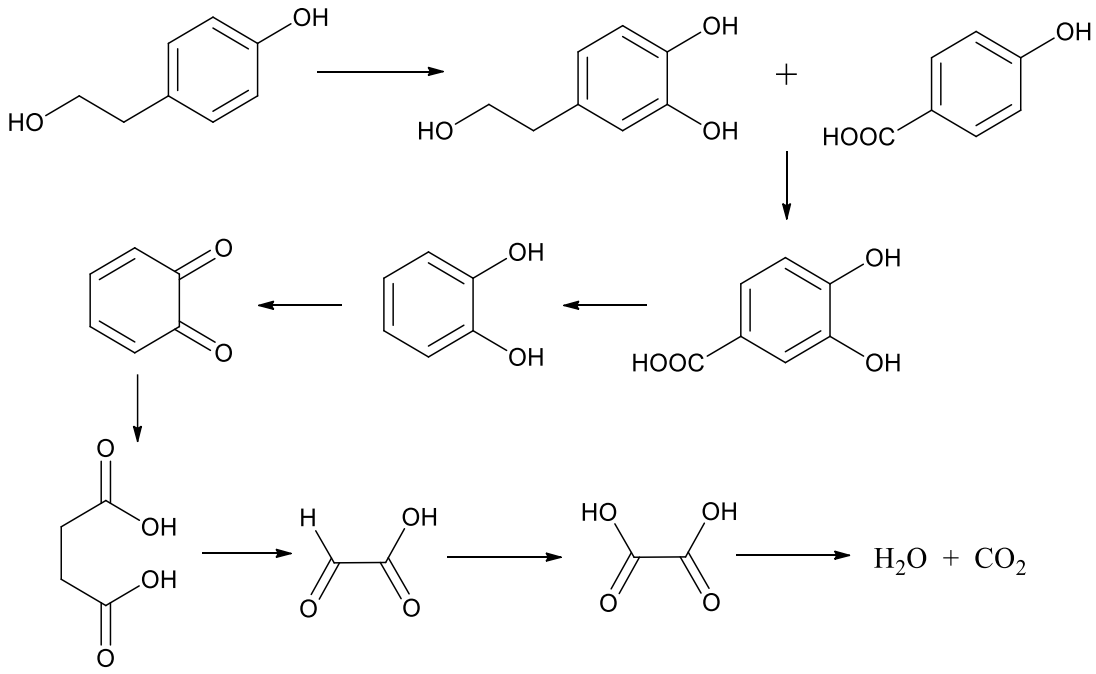

1. BATCH CONDITIONS

1.1 Powder study

After optimization of the reaction conditions, the most optimal ones were the following: Cu-MOF-808 NPs (5 mg, 0.003 mmol, 22 wt% cat Cu) were added to a non-stirred solution of

TyrOH (5 mL, 0.018 mmol, 500 mg·L^{-1} in distilled water) and H_2O_2 (27 mg, 0.240 mmol, 30 % in water) for 180 min at 60 ºC and pH 6 natural of the solution.[10] The beginning of the reaction (t = 0) is determined to be when the catalyst and H_2O_2 are added. After 120 min, the mixture with a yellow color was centrifugated using a Hettich MIKRO 200 centrifuge. Then, the liquid decanted was diluted and extracted with ethyl acetate to eliminate the rest of the copper and H_2O_2. The samples were then analyzed by UV-Visible spectroscopy at RT using an Agilent 8453 system at 279 nm with a detection limit of 10 mg·L^{-1} (Figure S13.1). The difference between the TyrOH removal, and the TyrOH released is the TyrOH degraded. The amount of TyrOH degraded was 90 %.

Blank experiments for the study of degradation were performed in the presence of H_2O_2 and MOF-808 pristine (Figure S13.2).

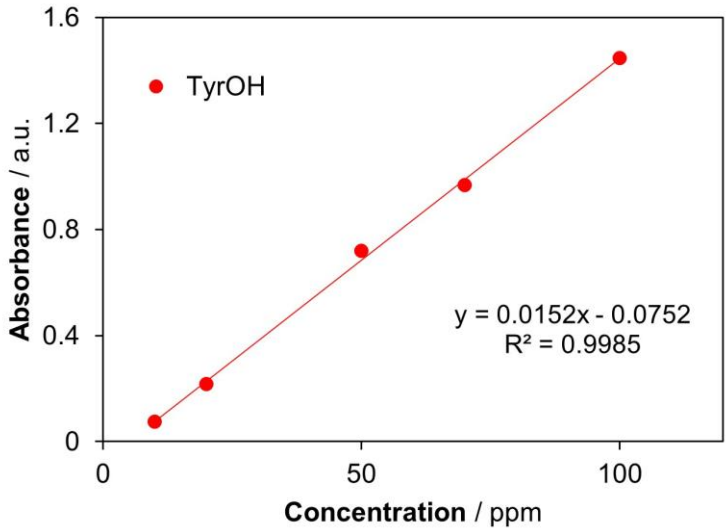

Figure S13.1. Calibration line for TyrOH in ethyl acetate as solvent.

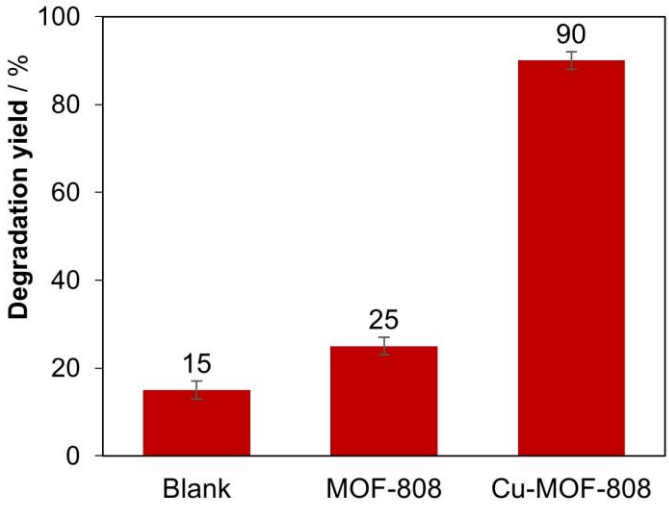

Figure S13.2. Catalytic degradation, over 5 mL of TyrOH 500 mg·L^{-1}.

Recyclability tests: The catalytic activity of Cu-MOF-808 NPs was observed to decline after four cycles of reuse (Figure S13.3). The MOF samples were recovered by washing them with water and acetone and subsequently drying them at 60 ºC overnight. XRD data were collected on the MOF samples after the final catalytic cycle to evaluate their crystallinity, purity, and recyclability (Figure S7.2). Additionally, FTIR (Figure S8.2) and ICP analyses (Table S13.1)

were performed. It was found that the deactivation of the catalyst was linked to the leaching of copper, which contributed homogeneously to the reactions. This was confirmed through hot filtration experiments, wherein the catalyst was removed after 30 minutes of reaction, but the same conversion yields were still achieved.

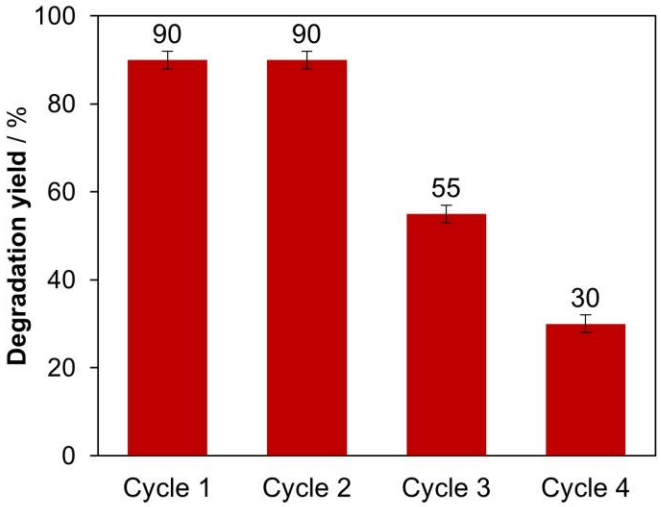

Figure S13.3. Recyclability tests for Cu-MOF-808 NPs.

1.2 Membrane study

Cu-MOF-808@PVDF (33 mg, 22 wt% cat Cu) was added to a non-stirred solution of TyrOH (5 mL, 0.018 mmol, 500 mg·L^{-1} in distilled water) and H_2O_2 (27 mg, 0.240 mmol, 30 % in water) for 180 min at 60 ºC and pH 6 natural of the solution. The beginning of the reaction (t = 0) is determined to be when the catalyst and H_2O_2 were added. After 180 min the reaction was stopped, the membrane was removed, and the mixture had a yellowish color. Then, the liquid was extracted with ethyl acetate to isolate the rest of the organic pollutants. The samples were analyzed by UV-Visible spectroscopy at RT using an Agilent 8453 system at 279 nm. The amount of H_2O_2 degraded was 90 %.

Blank experiments for the study of degradation were performed in the presence of PVDF and MOF-808@PVDF (Figure S13.4).

Recyclability tests: Cu-MOF-808@PVDF membrane was reused for up to 4 cycles. After recovery, the membranes were washed with water and dried with paper. ICP analyses were collected on the materials after the last catalytic cycle (Table S13.1) after the 4 cycles with a great improvement.

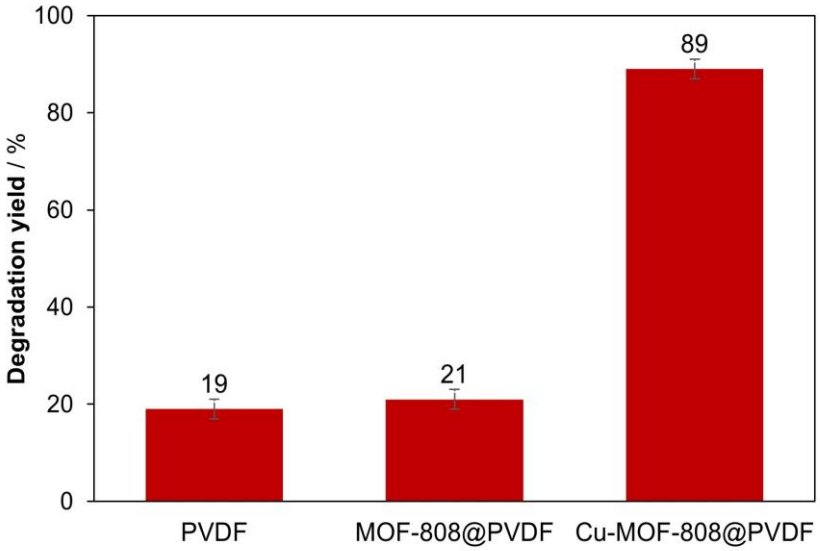

Figure S13.4. Membrane catalytic degradation, over 5 mL of TyrOH 500 mg·L^{-1}.

ICP analyses were performed with an Inducted Coupled Plasma Emission Spectrometer ICP PERKIN ELMER mod. OPTIMA 2100 DV. Samples (2 mg) were digested in 4 mL of a 1:1 H_2O_2:H_2SO_4 mixture (v:v) and taken to 10 mL in a volumetric flask volume with distilled water.

Table S13.1. ICP analyses of Cu-MOF-808 and Cu-MOF-808@PVDF MMM, before and after the cycles of the catalysis.

Compound	**Cu-MOF-808**	
	Cu atoms per Zr_6 cluster	% Cu loss/leaching in each cycle
NPs Cu-MOF-808 after catalysis	1.05	66
Cu-MOF-808@PVDF after catalysis	2.13	32

2. FLOW CONDITIONS

The use of a Mixed Matrix Membrane (MMM) based on MOF has the potential to address the different issues that are commonly encountered using powders in continuous flow chemistry. To this end, a flow reactor was designed to carry the catalytic reaction by pumping a feed solution through the membrane Cu-MOF-808@PVDF under a continuous model (Scheme S13.2). The reactor is a stainless catalytic membrane reactor with a residence time of 80 min, this was calculated from the following formula where the flow rate is 0.15 mL·min^{-1} and the volume of the reactor is 12 mL. [11]

$$Residence\ time\ \tau_r\ (\mathrm{min}) = \frac{Volume\ of\ reactor\ (mL)}{Output\ volumetric\ flow\ rate\ (mL \cdot min^{-1}\ )}$$

The reactor was placed in a water bath at 60°C. Using a NE-1000 syringe pump, distilled water was initially pumped through the nanoporous Cu-MOF-808@PVDF membrane. Subsequently, once the reactor was filled, we introduced the aqueous solution of TyrOH (500 mg·L-1 in distilled water) and H_2O_2 (13 equivalents) until reaching a steady state, maintaining a constant flow of 0.15 mL·min-1 (Scheme S13.3). The solution collected at the outlet was periodically recovered every 4 mL (equivalent to 20 min) and monitored via UV–Vis absorption spectroscopy. The substrate was degraded as shown by UV absorption, the pic of TyrOH at 279 nm decreases in absorbance. The continuous conversion of TyrOH, reaching approximately 50 %, persisted for over 5 hours. This duration corresponds to the treatment of 50 mL of solution (with a flux of 0.15 mL·min^{-1}), without observable deactivation (Figure S13.6), and the slightly gradual drop of the conversion rates after 5 h of high conversion could be attributed to the deactivation of the catalysts (TON = 0.95 and TOF = 0.19 h^{-1}).

Scheme S13.2. Illustration of the reactor operation.

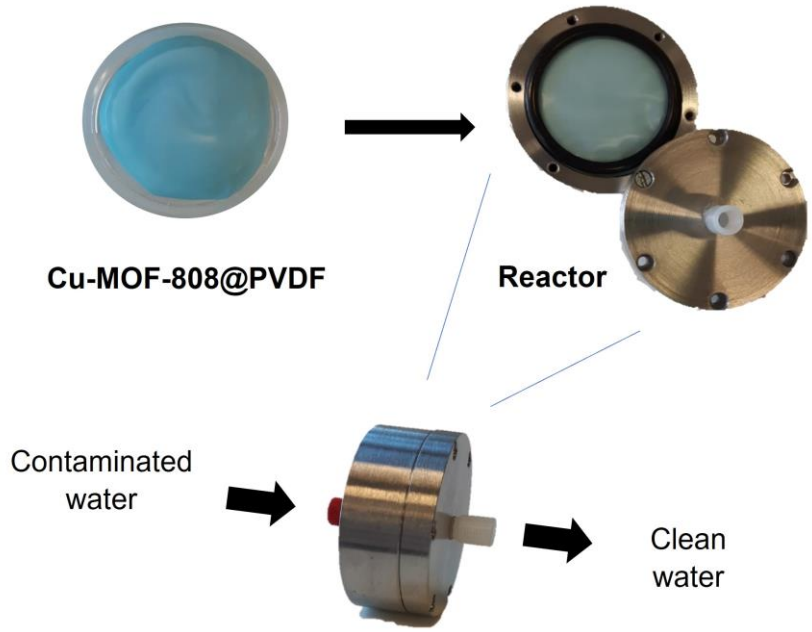

Scheme S13.3. Scheme (A) and illustration (B) of the membrane catalysis testing procedure.

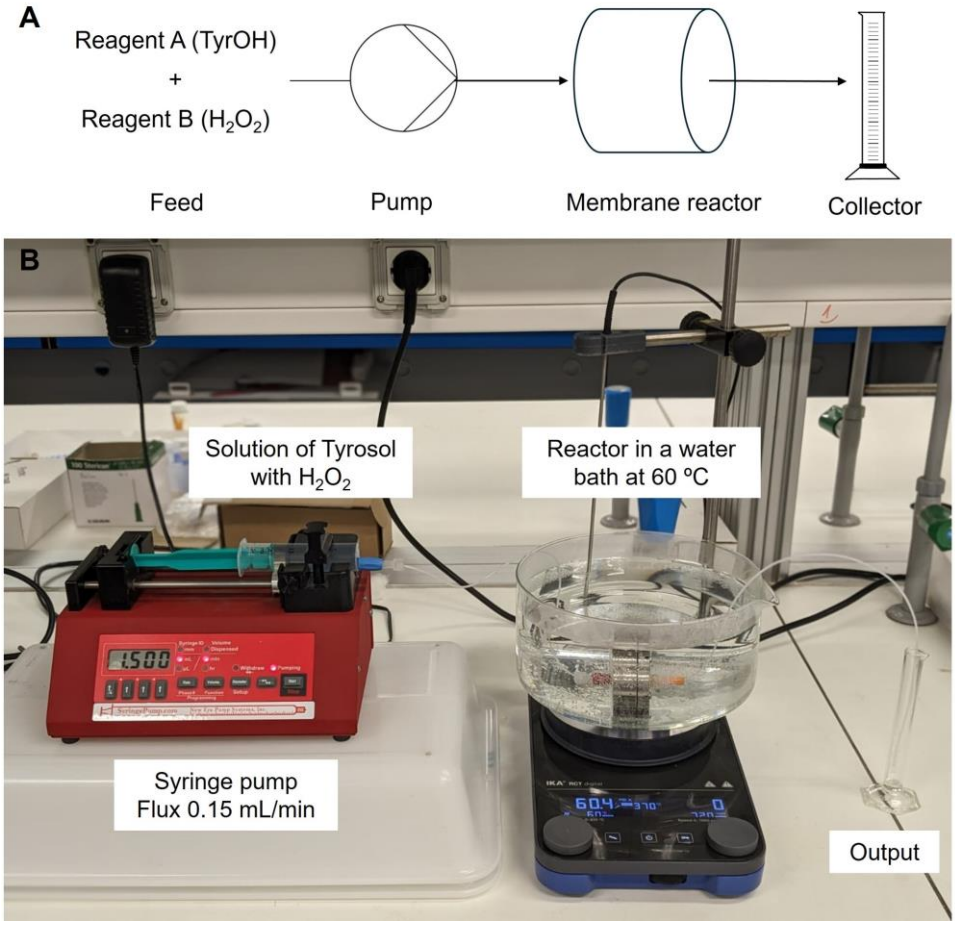

Blank experiments for the study of degradation were performed in the presence of H_2O_2 and MOF-808 pristine obtaining a conversion yield of around 20 % for both (Figure S13.5).

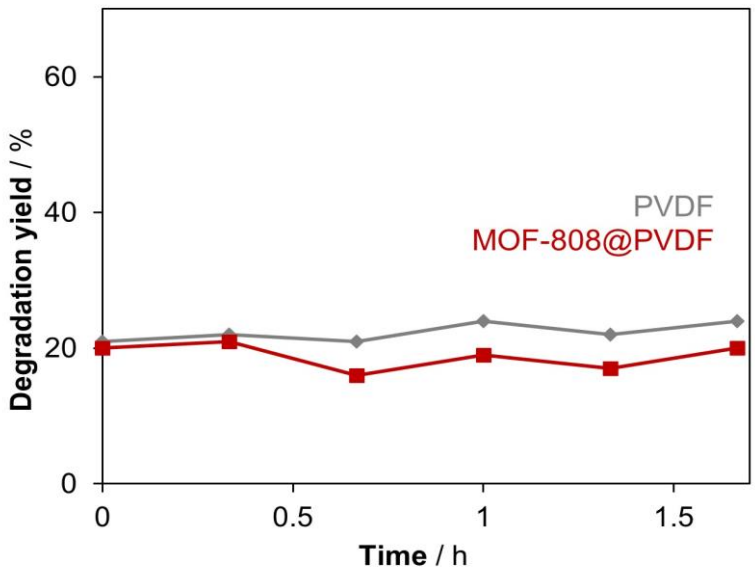

Figure S13.5. Catalytic degradation in flow, over 500 mg·L^{-1} TyrOH. Blank experiments.

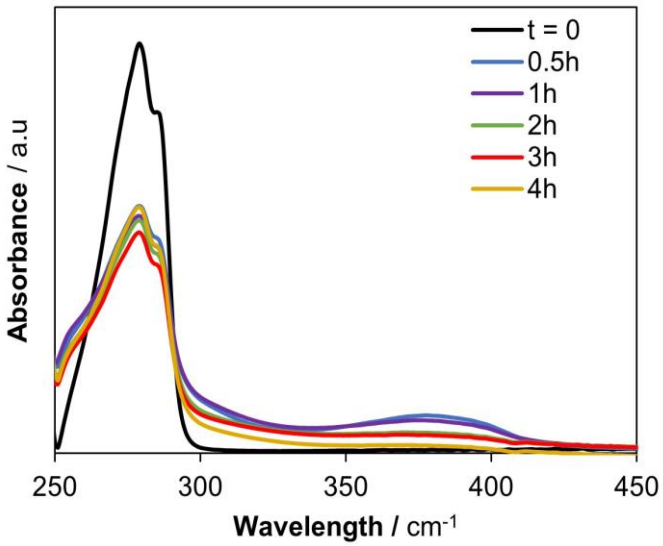

Figure S13.6. UV spectra of the catalytic degradation in flow, over 500 mg·L^{-1} TyrOH.

After recovery, the membranes were washed with water and dried with paper. XRD data were collected after the 8 h of flow reaction to evaluate crystallinity and purity after the process (Figure S7.3). FTIR (Figure S8.3) and ICP analyses (Table S13.2) were also made to these membranes. In addition, PDF and EXAFS experiments were carried out on these samples to better understand the catalytic pathway.

Table S13.2. ICP analyses of the Cu-MOF-808@PVDF MMM, after the flow catalysis.

Compound	**Cu-MOF-808**	
	Cu atoms per Zr_6 cluster	*%Cu loss/leaching*
Cu-MOF-808@PVDF after 1h catalysis	3.0	4
Cu-MOF-808@PVDF after 5h catalysis	2.4	20

3. COMPARATIVE ANALYSES

The Cu-BTC NPs were synthesized following a reported procedure mixing $Cu(NO_3)_2 \cdot 3H_2O$ with trimesic acid in dimethyl sulfoxide and then reprecipitating it in EtOH, yielding a blue powder.[12]

The Cu-BTC NPs were used as a catalyst in the Fenton reaction in the same conditions as the Cu-MOF-808 NPs. Cu-BTC (2 mg, 0.003 mmol, 22 wt% cat Cu) NPs were added to a non-stirred solution of TyrOH (5 mL, 0.018 mmol, 500 mg·L^{-1} in water) and H_2O_2 (27 mg, 0.240 mmol, 30% in water) for 180 min at 60 ºC. The observation was that when the reaction was finished the MOF has been dissolved, and there was a weight loss of 95 % of the catalyst.

In addition, flow experiments were carried out. The membrane Cu-BTC@PVDF was prepared with the same quantity of copper as in the Cu-MOF-808@PVDF. Then, the reaction was performed following the same procedure as before. The result obtained was the same conversion as for the Cu-MOF-808@PVDF but with higher leaching (Table S13.3) since the MOF decomposes (Figure S13.7).

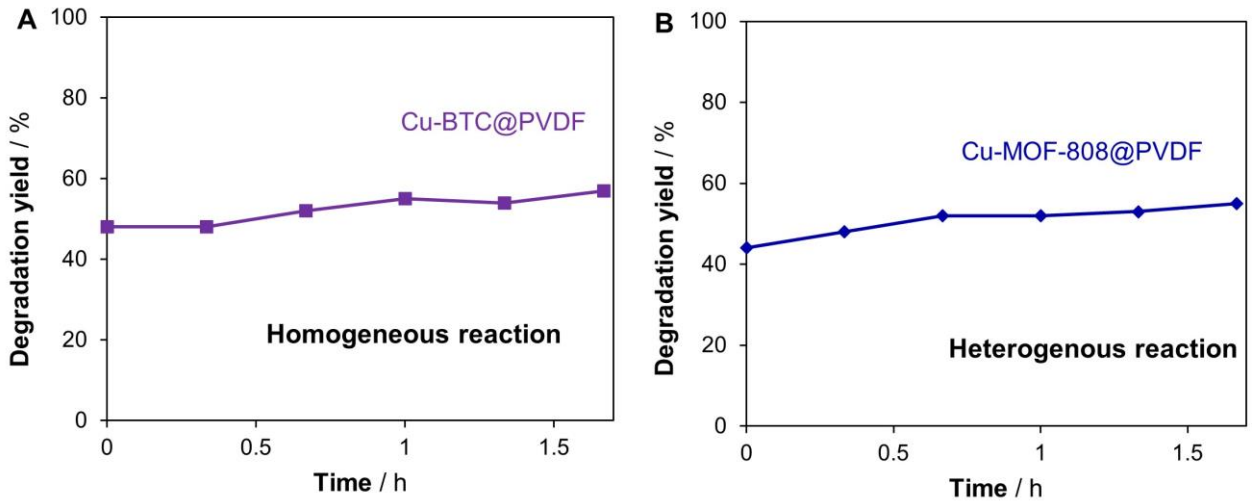

Figure S13.7. Catalytic degradation in flow for the different copper membranes over TyrOH. (A) With homogeneous contribution in the catalysis. (B) Heterogeneous catalysis.

Table S13.3. ICP analyses of the copper MMM after the flow catalysis.

Compound	***%Cu loss/leaching after 1h of flow reaction***
Cu-MOF-808@PVDF	4
Cu-BTC@PVDF	32

Table S13.4. Comparison of copper heterogeneous catalyst used in Fenton reactions.

Material	*Fenton reaction*	*Reagents*	*Conditions*	*Yield*	*Leaching*	*Ref*
FeCu@C MOF composite	Sulfamethazine degradation	20 mg·L^{-1} STM 25 wt% cat M 20 eq H_2O_2	25 ºC, pH=3, batch	100 % yield 1.6 mg degraded	70 wt%	[13]
CuO nanosheets	Photo Phenol degradation	50 mg·L^{-1} PhOH 27 wt% cat Cu 200 eq H_2O_2	30 ºC, pH= 12, batch	100 % yield 3.0 mg degraded	9 wt%	[14]
Cu-embedded alumina	Rhodamine B degradation	10 mg·L^{-1} RhB 500 wt% cat Cu 1000 eq H_2O_2	50 ºC, pH= 5, batch	98.5 % yield 1.0 mg degraded	0.9 wt%	[15]
Copper-supported pillared clay	Tyrosol degradation	500 mg·L^{-1} TyrOH 64 wt% cat Cu 19 eq H_2O_2	2h, 60 ºC, pH=6 nat. sol, flow	85-60 % yield 21.8 mg degraded	2.5 wt% (at 25 ºC)	[10]
Cu-BTC	Tyrosol degradation	500 mg L^{-1} TyrOH 22 wt% cat Cu 13 eq H_2O_2	3 h, 60 ºC, pH=6 nat. sol., batch	Homogeneous catalysis	100 wt%	This work
Cu-MOF-808	Tyrosol degradation	500 mg L^{-1} TyrOH 22 wt% cat Cu 13 eq H_2O_2	3 h, 60 ºC, pH=6 nat. sol., batch	90 % yield 2.3 mg degraded	60 wt%	This work
Cu-BTC @PVDF	Tyrosol degradation	500 mg·L^{-1} TyrOH 22 wt% cat Cu 13 eq H_2O_2	2 h, 60 ºC, pH=6 nat. sol., flow	50 % yield (partly homogeneous) 4.5 mg degraded	32 wt%·h^{-1}	This work
Cu-MOF-808 @PVDF	Tyrosol degradation	500 mg·L^{-1} TyrOH 22 wt% cat Cu 13 eq H_2O_2	5 h, 60 ºC, pH=6 nat. sol., flow	50 % yield 11.3 mg degraded	4 wt%·h^{-1}	This work

Water permeation study. The Cu-MOF-808@PVDF membranes exhibit high porosity, resulting in a significantly high water permeation rate. To demonstrate their long-term stability and the absence of a fouling effect, we measured their permeance value immediately after preparation and 8 months later. The membranes were initially immersed in distilled water for 1 hour and then measured using the Sterlitech HP4750 High Pressure Stirred Cell. Permeance was calculated using the following equation, where the pressure variance was 1 bar and the area 1.2x10^{-3} m^2. [16] The results are summarized in Table S13.5:

$$Permeance = \frac{V\ (L)}{\Delta P\ (bar) \cdot A\ (m^2) \cdot t\ (h)}$$

Table S13.5. Permeance values of the membranes over time.

Membrane	*Permeation (L·m^{-2}·bar^{-1}·h^{-1})*
Cu-MOF-808@PVDF	18800
Cu-MOF-808@PVDF after 8 months	11071

Therefore, although a slight decrease in the permeation value is noticeable over time, the high values indicate that fouling is negligible. Consequently, the membrane remains suitable for use even after an extended period.

References

1 H. Furukawa, F. Gándara, Y. B. Zhang, J. Jiang, W. L. Queen, M. R. Hudson and O. M. Yaghi, *J Am Chem Soc*, 2014, **136**, 4369–4381.

2 I. del Castillo-Velilla, A. Sousaraei, I. Romero-Muñiz, C. Castillo-Blas, A. S. J. Méndez, F. E. Oropeza, V. A. de la Peña O'Shea, J. Cabanillas-González, A. Mavrandonakis and A. E. Platero-Prats, *Nat Commun*, 2023, **14**, 2506–2516.

3 B. Ravel and M. Newville, *J Synchrotron Radiat*, 2005, **12**, 537–541.

4 M. Basham, J. Filik, M. T. Wharmby, P. C. Y. Chang, B. el Kassaby, M. Gerring, J. Aishima, K. Levik, B. C. A. Pulford, I. Sikharulidze, D. Sneddon, M. Webber, S. S. Dhesi, F. Maccherozzi, O. Svensson, S. Brockhauser, G. Náray and A. W. Ashton, *J Synchrotron Radiat*, 2015, **22**, 853–858.

5 P. Juhás, T. Davis, C. L. Farrow and S. J. L. Billinge, *J Appl Crystallogr*, 2013, **46**, 560–566.

6 S. Navalon, M. Alvaro and H. Garcia, *Appl Catal B*, 2010, **99**, 1–26.

7 A. D. Bokare and W. Choi, *J Hazard Mater*, 2014, **275**, 121–135.

8 S. Ammar, M. A. Oturan, L. Labiadh, A. Guersalli, R. Abdelhedi, N. Oturan and E. Brillas, *Water Res*, 2015, **74**, 77–87.

9 A. Azizi, M. Abouseoud and A. Amrane, *Nat Environ Pollut Technol*, 2017, **16**, 321–330.

10 R. Ben Achma, A. Ghorbel, A. Dafinov and F. Medina, *Appl Catal A Gen*, 2008, **349**, 20–28.

11 A. J. Niemi, *Pergamon Press*, 1977, **28**, 855-860.

12 N. A. A. Sani, W. J. Lau and A. F. Ismail, *RSC Adv*, 2015, **5**, 13000–13010.

13 J. Tang and J. Wang, *Chem Eng J*, 2019, **375**, 122007–122018.

14 M. Fang, R. Zheng, Y. Wu, D. Yue, X. Qian, Y. Zhao and Z. Bian, *Environ Sci: Nano*, 2019, **6**, 105–114.

15 Y. Sheng, Y. Sun, J. Xu, J. Zhang and Y. F. Han, *AIChE Journal*, 2018, **64**, 538–549.

16 L. Paseta, M. Navarro, J. Coronas and C. Téllez, *J Ind Eng Chem*, 2019, **77**, 344–354.